



8-2005

Pitot Tube and Wind Tunnel Studies of the Flow Induced by One Atmosphere Uniform Glow Discharge (OAUGDP[®]) Plasma Actuators using a Conventional and an Economical High Voltage Power Supply

Manish Yadav

University of Tennessee - Knoxville, manish.yadav@gmail.com

Recommended Citation

Yadav, Manish, "Pitot Tube and Wind Tunnel Studies of the Flow Induced by One Atmosphere Uniform Glow Discharge (OAUGDP[®]) Plasma Actuators using a Conventional and an Economical High Voltage Power Supply." Master's Thesis, University of Tennessee, 2005.

https://trace.tennessee.edu/utk_gradthes/935

This Thesis is brought to you for free and open access by the Graduate School at Trace: Tennessee Research and Creative Exchange. It has been accepted for inclusion in Masters Theses by an authorized administrator of Trace: Tennessee Research and Creative Exchange. For more information, please contact trace@utk.edu.

To the Graduate Council:

I am submitting herewith a thesis written by Manish Yadav entitled "Pitot Tube and Wind Tunnel Studies of the Flow Induced by One Atmosphere Uniform Glow Discharge (OAUGDP[®]) Plasma Actuators using a Conventional and an Economical High Voltage Power Supply." I have examined the final electronic copy of this thesis for form and content and recommend that it be accepted in partial fulfillment of the requirements for the degree of Master of Science, with a major in Electrical Engineering.

J. Reece Roth, Major Professor

We have read this thesis and recommend its acceptance:

Leon Tolbert, Mostafa Howlader

Accepted for the Council:

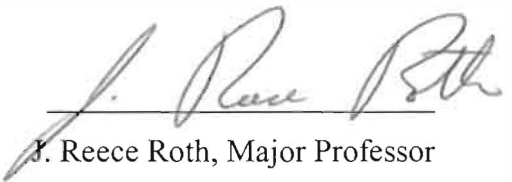
Dixie L. Thompson

Vice Provost and Dean of the Graduate School

(Original signatures are on file with official student records.)


To the Graduate Council:

I am submitting herewith a thesis written by Manish Yadav entitled "Pitot Tube and Wind Tunnel Studies of the Flow Induced by One Atmosphere Uniform Glow Discharge (OAUGDP[®]) Plasma Actuators using a Conventional and an Economical High Voltage Power Supply". I have examined the final paper copy of this thesis for form and content and recommend that it be accepted in partial fulfillment of the requirements for the degree of Master of Science, with a major in Electrical Engineering.




J. Reece Roth, Major Professor

We have read this thesis and recommend its acceptance:




Leon Tolbert



Mostafa Howlader

Accepted for the Council:



Vice Chancellor and Dean of Graduate Studies

**PITOT TUBE AND WIND TUNNEL STUDIES OF THE FLOW INDUCED
BY ONE ATMOSPHERE UNIFORM GLOW DISCHARGE (OAUGDP[®])
PLASMA ACTUATORS USING A CONVENTIONAL AND AN
ECONOMICAL HIGH VOLTAGE POWER SUPPLY**

**A Thesis Presented for
the Master of Science Degree
The University of Tennessee, Knoxville**

Manish Yadav

August – 2005

PLEASE DO NOT WRITE ON THE FRONT COVER

DEDICATION

BY ONE WHO RECEIVED THE DEGREE OF DOCTOR OF PHILOSOPHY
This work is dedicated to my parents for their tireless encouragement and support.

PLEASE RETURN TO THE LIBRARY

UNIVERSITY OF CALIFORNIA, LOS ANGELES

A Thesis Submitted to

the Faculty of the Department of

Psychology in partial fulfillment of the requirements for the

Ph.D. degree

by
M. S. Yeh

ACKNOWLEDGEMENT

Thanks are due first to my supervisor, Professor J. Reece Roth, for his great insights, perspectives and guidance throughout my stint as a graduate student at the University of Tennessee. My sincere thanks go to Professor Leon Tolbert and Professor Mostafa Howlader for serving as my committee members. I also thank my colleagues at the UT Plasma Sciences Laboratory for their excellent cooperation. I am grateful to Mr. Steve Wilkinson for his help during the work done at the NASA Langley Research Center. This work was supported in part by AFOSR contract AF F49620-01-1-0425 (ROTH), Dr. John Schmisser, Program Manager.

I thank my friends both here in United States and back home in India, who have not been mentioned here personally in making this educational process a success. Last but not the least, I thank my family members for all their love and encouragement. I could not have made it without your support.

ABSTRACT

The aerodynamic applications of plasma science is a field of growing interest. Investigations using various approaches have been initiated by several research groups that are designed to manipulate the aerodynamic boundary layer and to re-attach the flow to airfoils. EHD (ElectroHydroDynamic) flow control has proven at least as effective as other methods of boundary layer flow control. In the EHD approach, glow discharge plasma actuators are placed on the wings and fuselage of the aircraft, or on the turbine blades in the engine, to influence the boundary layer flow. This thesis is concerned with plasma actuators based on the OAUGDP[®] (One Atmosphere Uniform Glow Discharge Plasma). An actuator consists of two conducting electrodes separated by a dielectric plate. When a sufficiently high RF voltage is supplied to the electrodes, the surrounding air ionizes and forms plasma in regions in which the electric field is above approximately 10 kV/cm. The ionized air, in the presence of an electric field gradient, produces a body force on the neutral gas flow.

This work is concerned with two EHD effects: paraelectric flow acceleration and peristaltic flow acceleration. In the paraelectric mode, electric field gradients act on the net charge density of plasma, and the plasma drags the neutral gas along with it due to ion-neutral and electron-neutral Lorentzian collisions. In the peristaltic mode, successive actuators are energized with the same voltage, but increasing phase angles. The first part of this thesis describes experiments at the NASA Langley Research Center, Hampton, VA in the 7 x 11

Inch Low Speed Wind Tunnel in which Pitot tube velocity profile measurements and smoke flow visualization tests were conducted.

The second part of this thesis describes the development of a low cost power supply to energize OAUGDP[®] plasma actuators. The power supply consists of automotive ignition coil transformers, audio amplifiers, and a DC battery. Using this power supply, plasma actuators were energized at voltages up to 8 kV, and at frequencies between 0.5 and 8 kHz. This thesis also presents illustrative piezoelectric flow acceleration data obtained using the low-cost power supply.

TABLE OF CONTENTS

Chapter 1: INTRODUCTION

1.1	Plasma.....	1
1.2	History of Electrical Discharges.....	1
1.3	Need for Glow Discharge Plasma Sources at One Atmosphere of Pressure.....	2
1.4	One Atmosphere Plasma Sources.....	2
1.5	The OAUGDP® (One Atmosphere Uniform Glow Discharge Plasma).....	3
1.6	EHD (Electrohydrodynamic) Flow Control.....	4
1.6.1	Peraelectric Flow Acceleration.....	6
1.6.2	Peristaltic Flow Acceleration.....	9

Chapter 2: ELECTRODE GEOMETRIES

2.1	Parallel Plate Plasma Reactors.....	12
2.2	Coplanar Plasma Actuators.....	12
2.3	Asymmetric Electrode Configuration.....	14
2.3.1	Peraelectric Plasma Actuators.....	16
2.3.2	Peristaltic Plasma Actuators.....	20

Chapter 3: EXPERIMENTAL SET-UP

3.1	The Power Supply.....	24
3.1.1	Power Supply for Peraelectric Plasma Actuators.....	26
3.1.2	Peristaltic Plasma Actuator Power Supply.....	27
3.2	Polyphase Signal Generator (LabVIEW™).....	29
3.3	The Wind Tunnel.....	32
3.4	Pitot Tube System.....	32
3.5	Smoke Wire Flow Visualization System.....	36

Chapter 4: EXPERIMENTAL RESULTS

4.1	Boundary Layer Velocity Profiles.....	38
4.2	Boundary Layer Profile with Plasma Off.....	41
4.3	Effect of Frequency.....	42
4.4	Effect of Number of Electrodes Energized.....	44
4.5	Effect of Applied RF Voltage.....	45
4.6	Smoke Flow Visualization Tests.....	46
4.6.1	Smoke Flow Visualization using a Peraelectric Panel.....	48
4.6.2	Smoke Flow Visualization using a Peristaltic Panel.....	48

Chapter 5: LOW COST POWER SUPPLY

5.1	Components of the Low Cost Power Supply.....	54
5.1.1	Audio Amplifiers.....	54
5.1.2	Automotive Ignition Coils.....	57
5.1.3	DC Battery.....	58
5.2	Experimental Set-up.....	60
5.3	Experimental Results.....	62
5.4	Advantages of the Low Cost Power Supply.....	63

Chapter 6: SUMMARY AND DISCUSSION.....66

REFERENCES.....67

VITA.....72

LIST OF FIGURES

Figure 1.1: Parallel plate OAUGDP [®] reactor.....	5
Figure 1.2: Asymmetric panel with staggered lower electrodes.....	7
Figure 1.3: Paraelectric flow acceleration in an electric field gradient.....	7
Figure 1.4: Polyphase power supply used to energize a peristaltic panel.....	10
Figure 2.1: Features of the normal glow discharge during half the RF cycle.....	13
Figure 2.2: Asymmetric panel configuration.....	15
Figure 2.3: Panel with asymmetric electrodes used for paraelectric flow acceleration.....	16
Figure 2.4: Paraelectric panel – electrodes on the upper surface and metallic sheet electrode on the lower surface of the panel.....	17
Figure 2.5: Symmetric paraelectric actuator – electrodes on the upper and lower surface of the panel.....	18
Figure 2.6: Asymmetric paraelectric panel used for flow acceleration.....	18
Figure 2.7: Aluminum oxide (Al ₂ O ₃) paraelectric panel (dimensions in mm).....	19
Figure 2.8: Peristaltic flow acceleration due to traveling electrostatic wave.....	20
Figure 2.9: Peristaltic flow acceleration in a combined paraelectric and peristaltic acceleration.....	21
Figure 2.10: Aluminum oxide (Al ₂ O ₃) pure peristaltic panel (dimensions in mm).....	22
Figure 2.11: Aluminum oxide (Al ₂ O ₃) combined paraelectric and peristaltic panel (dimensions in mm).....	23
Figure 3.1: Digital image of the power supply composed of Powertron [™] amplifiers and high voltage transformers.....	25
Figure 3.2: Paraelectric plasma actuator energized by the power supply.....	26

Figure 3.3: Block diagram of the power supply used to drive peristaltic plasma actuators.....	28
Figure 3.4: Schematic of the polyphase signal generator.....	30
Figure 3.5: Front panel of the LabVIEW polyphase generator program.....	31
Figure 3.6: Schematic of the low speed wind tunnel.....	33
Figure 3.7: Digital image of the NACA 0015 airfoil with OAUGDP electrode strips mounted in the NASA Langley Research Center's 7 X 11 Inch Low Speed Wind Tunnel.....	33
Figure 3.8: Experimental configuration of the Pitot tube system.....	34
Figure 3.9: Pitot tube positioner ATS100 series.....	35
Figure 3.10: Components of the smoke wire flow visualization system.....	37
Figure 4.1: Schematic drawing of an aluminum oxide panel, showing the position of the Pitot tube above the panel.....	39
Figure 4.2: Digital image of the Pitot tube and the aluminum oxide (Al_2O_3) panel mounted in the wind tunnel.....	40
Figure 4.3: Digital image of the opening of the Pitot tube.....	40
Figure 4.4: Schematic of the Pitot tube measurement system in the wind tunnel.....	41
Figure 4.5: Velocity profile with plasma off and wind tunnel free stream velocity of 3.95 m/sec.....	42
Figure 4.6: Flow velocity plotted as a function of applied RF frequency.....	43
Figure 4.7: Flow velocity plotted as a function of number of electrodes energized.....	44
Figure 4.8: Effect of voltage and the mode of EHD operation on the flow velocities.....	45
Figure 4.9: Effect of applied RF voltage and frequency on the flow velocities...	46
Figure 4.10: Experimental set-up for smoke flow visualization tests.....	47

Figure 4.11: Smoke flow visualization tests for paraelectric panel.....	49
Figure 4.12: Smoke flow visualization tests for pure peristaltic panel.....	51
Figure 4.13: Smoke flow visualization tests for combined paraelectric and peristaltic panel.....	53
Figure 5.1: SPL CRM300-2 audio amplifier.....	55
Figure 5.2: Automotive ignition coils.....	57
Figure 5.3: 12V DC battery.....	58
Figure 5.4: Battery charger.....	59
Figure 5.5: Schematic for the power supply system.....	60
Figure 5.6: Experimental configuration for the power supply system.....	61
Figure 5.7: OAUGDP actuator panels. (a) Plasma panel under normal illumination. (b) Plasma panel energized by the low cost power supply.....	62
Figure 5.8: Effect of applied voltage and frequency on the flow velocity.....	63

1. INTRODUCTION

1.1 Plasma

In 1879, Sir William Crookes categorized plasma as the fourth state of matter. In explanation, he noted that plasma is formed when heat is applied to a gas, after transformation from solid to liquid and then from a liquid to the gaseous state. In the plasma state, individual atoms break down into electrons and ions. Irving Langmuir circa 1928 gave a more detailed definition of plasma as an approximately electrically neutral collection of ions and electrons which may or may not contain a neutral background gas [1].

1.2 History of Electrical Discharges

Many scientists of the 19th century investigated the behavior of DC electrical discharges in gases. Sir Humphry Davy in 1808 produced a steady-state DC arc discharge in atmospheric air, followed by Michael Faraday, who developed the high voltage, low pressure DC electrical discharge tube circa 1830. J Plucker (1859) and J W Hittorf (1869) demonstrated the emergence of cathode rays from the negative electrode of such discharges, and the fluorescence effect it caused. In these classical low pressure electrical discharges, a filamentation instability (streamers) occurred when attempts were made to operate a glow discharge above a few Torr of pressure. The instability was usually accompanied by cathode heating, thermionic emission from the cathode, and a glow-to-arc transition [1].

1.3 Need for Glow Discharge Plasma Sources at One Atmosphere of Pressure

The plasma sources operating much below or above one atmosphere of pressure have significant disadvantages. Sources operating under vacuum have the added cost of purchasing and maintaining the vacuum system, and additional operating costs are associated with the batch processing of workpieces. Batch processing of workpieces is also required for plasma sources operating above 1 atm, and regulatory restrictions associated with the National Boiler Code make the enclosure design complex and expensive for operation above 3 atm. For these reasons, plasma sources operating at 1 atm generally produce industrially optimum operating conditions at low cost.

1.4 One Atmosphere Plasma Sources

In regions of high electric field near sharp points where electrically stressed gas is present, a corona discharge may exist if the electric field exceeds that for breakdown of the gas. Corona discharges have applications in electrostatic precipitators, xerography, modifying the surface properties of materials, and in air freshening. However, corona sources may produce such detrimental effects as formation of ozone, X-rays, NO₂ and nitric acid (in the presence of water vapor), and production of audible and RF noise. In addition, these sources are characterized by low production rates of active species and formation of corrosive active species that lead to degradation of electrodes and workpieces [2].

Another source that can be operated at one atmosphere is the Dielectric Barrier Discharge (DBD), generated in the space between two electrodes, each of which is covered with an insulating dielectric material. These sources are used for ozone production and increasing the surface energy of materials. However, these sources can produce ozone, audible noise, and radio frequency interference below a few MHz, and can cause pinhole damage of the workpiece and dielectric barrier. Also, the DBD is a filamentary plasma, which can lead to non-uniformity of effect when treating surfaces.

1.5 The OAUGDP[®] (One Atmosphere Uniform Glow Discharge Plasma)

Von Engle *et al* [3] made a major breakthrough in 1933 when they obtained normal glow discharges at 1 atm, by starting the discharge under vacuum and then gradually increasing the pressure to 1 atm. Among the limitations of this discharge were a requirement for aggressively cooled cathodes, and instability of the discharge with respect to the glow-to-arc transition at pressures approaching one atmosphere.

J.R. Roth and his co-workers at Plasma Sciences Laboratory at University of Tennessee operated the first One Atmosphere Uniform Glow Discharge Plasma in air using a parallel plate OAUGDP[®] reactor. This capacitively coupled plasma is generated between two electrodes, at least one of which is covered by a dielectric. This dielectric material is used to prevent RF arcs and to allow the build-up of surface charge, important to the operation of the plasma.

The OAUGDP[®] works on the principle of ion trapping. The critical frequency at which ions are trapped, and the uniform discharge is produced, is given by

$$\nu_0 \approx \frac{e V_{rms}}{\pi m \nu_c d^2} \text{ Hz} . \quad (1)$$

where ν_0 is the critical trapping frequency, m is the ion mass, V_{rms} is the rms voltage applied to the reactor plates, d is the distance between the plates, and ν_c is the ion collision frequency. When the plasma reactor configuration and the operating parameters are set to values consistent with Equation 1, the mobility drift of the ions in the oscillating electric field traps them between the electrodes during an RF cycle. Ion trapping is advantageous in that it prevents charge loss, and overheating of the cathode, which may lead to thermionic emission [4].

To demonstrate that the OAUGDP[®] displays the characteristics of a glow discharge plasma, Massines et al 1998 [5] and Ben Gadri [6] developed a one-dimensional computer simulation of a helium plasma. They observed all the features of a normal glow discharge in the OAUGDP[®] e.g. the cathode fall region, negative glow, Faraday dark space, and the positive column. These features are indicated schematically in Figure 1.1.

1.6 EHD (Electrohydrodynamic) Flow Control

EHD, by definition, is the study of the behavior of electrically charged fluids in the presence of electric fields. EHD flow control depends upon the

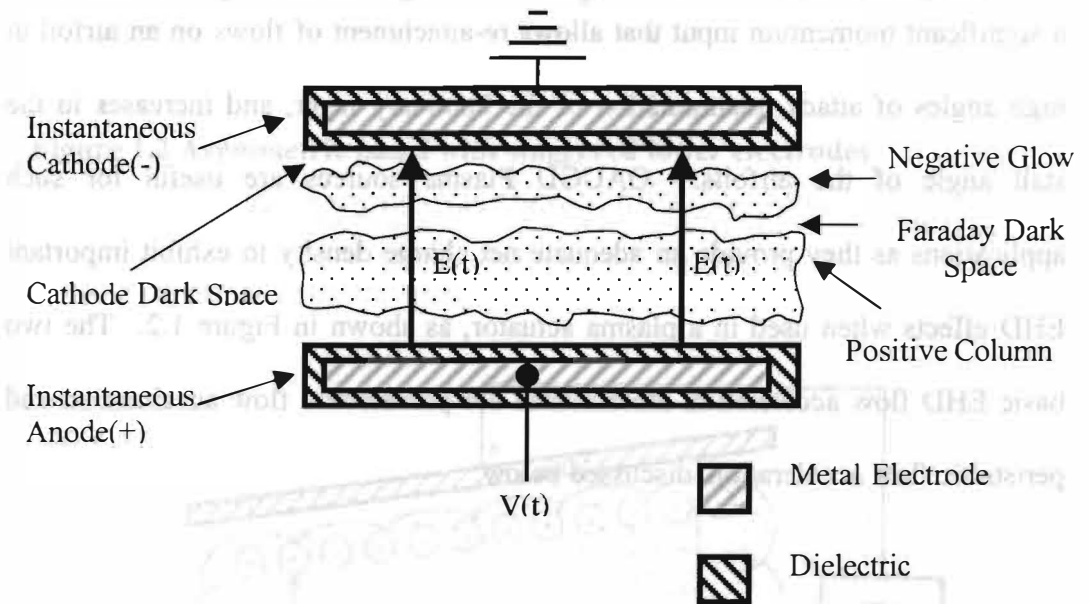


Figure 1.1 Parallel plate OAUGDP[®] reactor.

interaction between the partially ionized gas and the electric field. The resultant ion-neutral and electron-neutral Lorentzian collisions drag the neutral gas towards an increasing electric field gradient [1, 7]. The strong EHD coupling between the electric field in the plasma and flowing neutral gas in the boundary layer provides a significant momentum input that allows re-attachment of flows on an airfoil at high angles of attack, manipulation of the boundary layer, and increases in the stall angle of the airfoils. OAUGD Plasma sources are useful for such applications as they provide an adequate net charge density to exhibit important EHD effects when used in a plasma actuator, as shown in Figure 1.2. The two basic EHD flow acceleration mechanisms are paraelectric flow acceleration and peristaltic flow acceleration, discussed below.

1.6.1 Paraelectric Flow Acceleration

Electric field lines terminate on charged species or on charged conductors. As shown in Figure 1.3, in an electric field, charges of opposite polarity are pulled together. If a neutral gas is present, it, along with the plasma, moves towards the region of shorter electric field lines and stronger electric field gradient due to Lorentzian electron-neutral and ion-neutral collisions. By generating the OAUGDP[®] on a flat surface, significant EHD body forces can be exerted in the aerodynamic boundary layer above the surface [8, 9].

The flow accelerating effect of electron-neutral collisions is far less significant than that due to ion-neutral collisions. Though electrons possess a

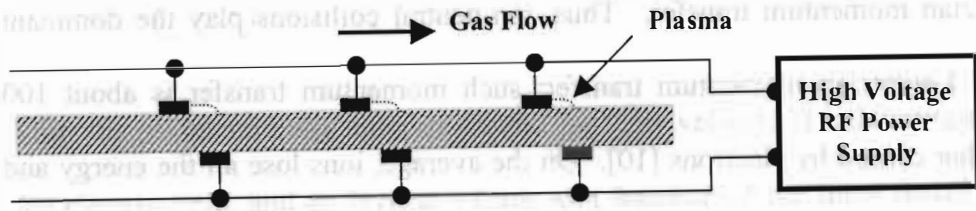


Figure 1.2 Asymmetric panel with staggered lower electrodes.

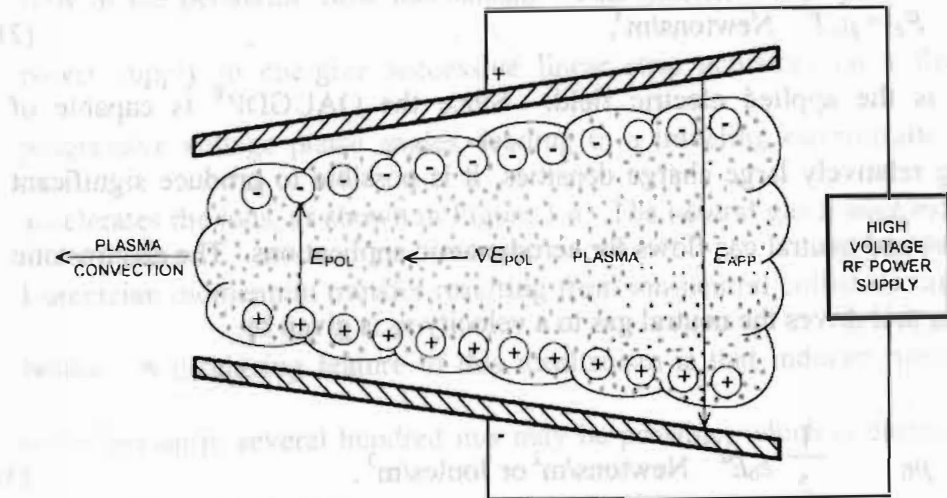


Figure 1.3 Paraelectric flow acceleration in an electric field gradient.

higher drift velocity than that of ions, their small mass leads to a much smaller Lorentzian momentum transfer. Thus, ion-neutral collisions play the dominant role in Lorentzian momentum transfer; such momentum transfer is about 100 times that caused by electrons [10]. On the average, ions lose all the energy and momentum that they gained since their last Lorentzian collision. Because of the low fractional ionization of the OAUGDP[®], Coulomb collisions between electrons and ions play an insignificant role in the momentum transfer.

The electrostatic body force on a plasma with a net charge density ρ_c is expressed as

$$F_E = \rho_c E \text{ Newtons/m}^3, \quad (2)$$

where E is the applied electric field. Since the OAUGDP[®] is capable of generating relatively large charge densities, it is possible to produce significant body forces and neutral gas flows for aerodynamic applications. The electrostatic pressure p_E that drives the neutral gas to a velocity v_0 is given by

$$p_E = \frac{1}{2} \epsilon_0 E^2 \text{ Newtons/m}^2 \text{ or Joules/m}^3. \quad (3)$$

The kinetic energy of a flow of velocity v_0 creates a stagnation pressure p_s which is also equal to the electrostatic pressure expressed by

$$p_s = \frac{1}{2} \rho v_0^2 = \frac{1}{2} \epsilon_0 E^2 \text{ Newtons/m}^2. \quad (4)$$

Using equation (4) above, the neutral gas flow velocity v_0 may be written

$$v_0 = E \left[\frac{\epsilon_0}{\rho} \right]^{1/2} \text{ meters/second} \quad (5)$$

Thus the paraelectrically induced neutral gas flow velocity is a linear function of the electric field, and an inverse square root function of the mass density of the neutral working gas.

1.6.2 Peristaltic Flow Acceleration

An electrostatic traveling wave is responsible for accelerating the gas flow in the peristaltic flow mechanism. This mechanism employs a polyphase power supply to energize successive linear strip actuators on a flat panel at progressive voltage phase angles, leading to a traveling electrostatic wave that accelerates the ions, as shown in Figure 1.4. The neutral gas is accelerated due to Lorentzian momentum transfer resulting from ion-neutral collisions, as explained before. A promising feature of this mechanism is that induced peristaltic flow velocities up to several hundred m/s may be possible, which is comparable with aircraft flight speeds [11].

As shown in Figure 1.4, individual actuator electrodes are energized with a phase angle that increases from left to right, giving rise to a traveling electrostatic wave moving from left to right. The electrodes are spaced L m apart, and each is energized by a single sequenced phase of the polyphase power supply output. When there are N electrodes per RF period placed on the panel, each

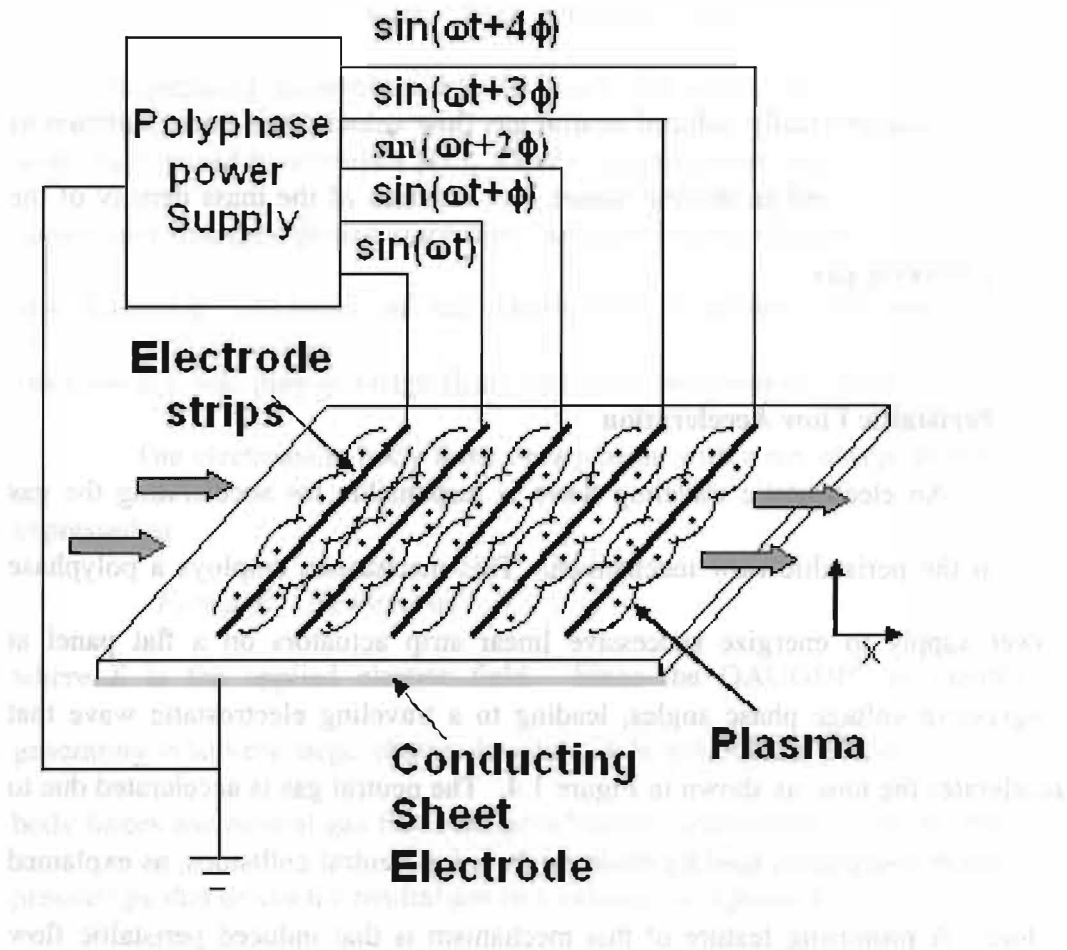


Figure 1.4 Polyphase power supply used to energize a peristaltic panel.

actuator electrode has a phase angle of $360^\circ/N$ with respect to the adjacent electrode. The voltage of the traveling wave, V , is expressed as

$$V = V_0 \sin(\omega t - kx) \quad \text{Volts,} \quad (6)$$

where k is the wavenumber of the electrostatic wave,

$$k = \frac{2\pi}{NL} \quad \text{m}^{-1}. \quad (7)$$

The phase angle Φ between adjacent electrode pairs is given by,

$$\Phi = \frac{360^\circ}{N}. \quad (8)$$

The maximum horizontal electric field of the traveling wave is

$$E_{max} = \frac{2\pi V_0}{NL} \quad \text{V/m,} \quad (9)$$

And the maximum ion-induced neutral convection velocity v_{oi} is

$$v_{oi} = \mu_i E_{max} = \frac{e}{M_i v_{in}} \times \frac{2V_0}{NL} \quad \text{m/s,} \quad (10)$$

where μ_i is the ion mobility and M_i is the ion mass.

2. ELECTRODE GEOMETRIES

2.1 Parallel Plate Plasma Reactors

A parallel plate plasma reactor operated as an OAUGDP[®] with dielectric coated electrodes was shown in Figure 1.1. The structures shown in Figure 1.1 reverse their sequence with each half cycle of the RF. This configuration, however, is not useful for aerodynamic flow control. Other actuator configurations similar to Figure 2.1 were tested at the UT Plasma Sciences Laboratory, where bare electrodes of opposite RF polarity were located on the same side of a dielectric panel. This configuration not only gave rise to sparking and tracking, but also the maximum time the panel would survive without breakdown was only 5-10 seconds.

2.2 Coplanar Plasma Actuators

Due to the lack of utility of the parallel plate configuration for aerodynamic applications, several approaches were tried at the UT Plasma Sciences Laboratory to produce OAUGD plasma on a flat panel. In panels designed early in 1995, bare electrodes were placed on the same side of a dielectric panel. This configuration, however, gave rise to tracking and sparking on the panel surface. Thereafter, panels were designed that had electrodes of different polarity on opposite sides of the panel.

To understand the coplanar actuator configuration, one can visualize that the upper electrode of a parallel plate reactor is flipped over and placed adjacent to the lower electrode to make them coplanar as in Figure 2.1.

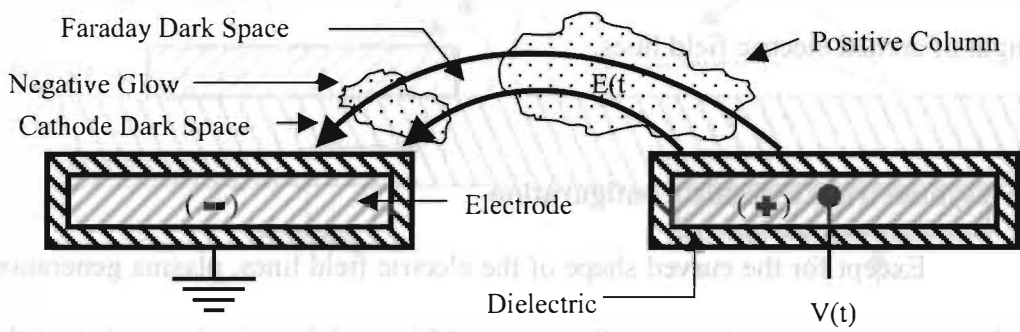


Figure 2.1 Features of the normal glow discharge during half the RF cycle.

Such a configuration is capable of providing a purely EHD coupling between the electric field in the plasma and the neutral gas in the boundary layer through Lorentzian collisions. The structures in the co-planar flat panel configuration used for aerodynamic flow control are illustrated in Figure 2.1. This configuration forms a flat layer of surface plasma. As shown in Figure 2.1, the structures of the normal glow discharge plasma are distributed along the length of arched electric field lines.

2.3 Asymmetric Electrode Configuration

Except for the curved shape of the electric field lines, plasma generation in the asymmetric, co-planer configuration of Figure 2.2 is similar to that of the parallel plate configuration. The strength of the electric field is greatest near the facing edges of the two electrodes, and decreases as the distance from the electrodes increases. For the first half cycle, illustrated in Figure 2.2, the dielectric behaves as an anode (pseudo anode), and the electrons, after being emitted from the instantaneous cathode on the left, travel towards the pseudo anode. These electrons collide with neutrals and lead to further ionization. During the second half cycle, the energy density in the (now positive column) plasma is less than that of the first half cycle [12]. The electrons possess energy comparable to the threshold ionization energy only in the cathode region. Due to the inability of the pseudo cathode (dielectric) to emit thermionic electrons, electrons decrease in number as they recombine.

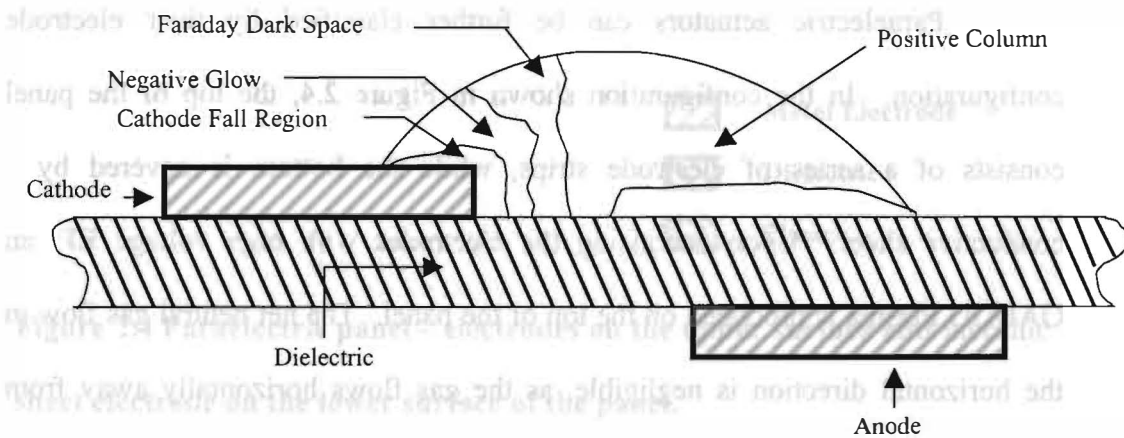


Figure 2.2 Asymmetric panel configuration.

2.3.1 Paraelectric Plasma Actuators

The gas flow induced by paraelectric actuator panels is due to the EHD paraelectric flow mechanism described in Section 1.6.1. The geometry of the paraelectric panel is shown in Figure 2.3.

Paraelectric actuators can be further classified by their electrode configuration. In the configuration shown in Figure 2.4, the top of the panel consists of a series of electrode strips, while the bottom is covered by a conductive sheet. Upon energizing the electrodes with high voltage RF, an OAUGD Plasma is produced on the top of the panel. The net neutral gas flow in the horizontal direction is negligible, as the gas flows horizontally away from *both* edges of each electrode. Though this panel is not of much utility for aerodynamic purposes, except to induce flat plate drag, it is useful for the diagnostic measurement of the OAUGD plasma parameters, and in the treatment of fabrics.

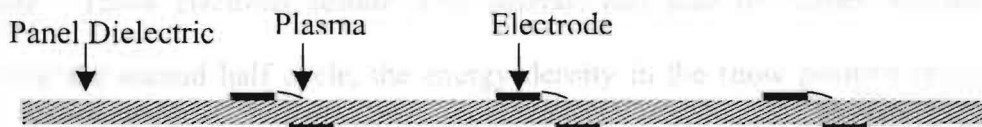


Figure 2.3 Panel with asymmetric electrodes used for paraelectric flow acceleration.

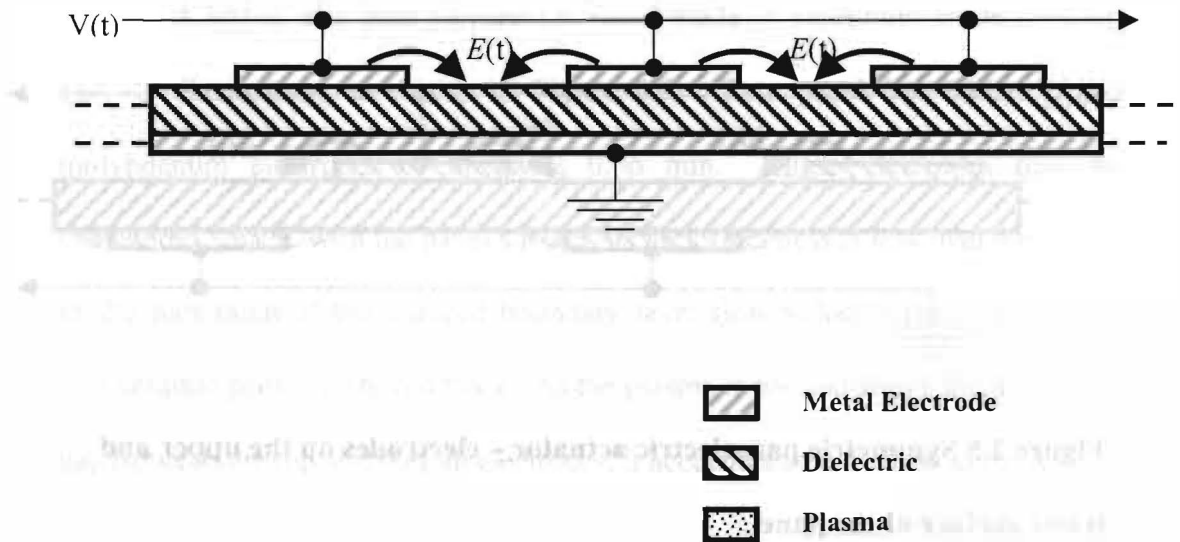


Figure 2.4 Paraelectric panel – electrodes on the upper surface and metallic sheet electrode on the lower surface of the panel.

Another configuration used for the surface treatment of fabrics and in inducing drag is shown in Figure 2.5. In this symmetric configuration, the upper and lower surfaces of the panel contain electrodes of opposite polarity, and a OAUGDP[®] is produced on both sides of the panel.

A configuration proposed for use in aerodynamic applications is shown in Figure 2.6 that is capable of accelerating the airflow above the surface of the panel to the right. This asymmetric paraelectric panel consists of electrodes of opposite polarity placed on the top and bottom surfaces of a dielectric panel. There is a small gap between the trailing edge of the top and the leading edge of the bottom electrodes.

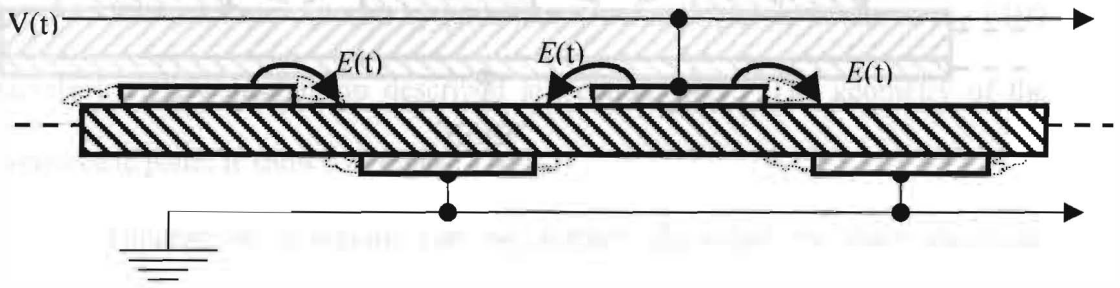


Figure 2.5 Symmetric paraelectric actuator – electrodes on the upper and lower surface of the panel.

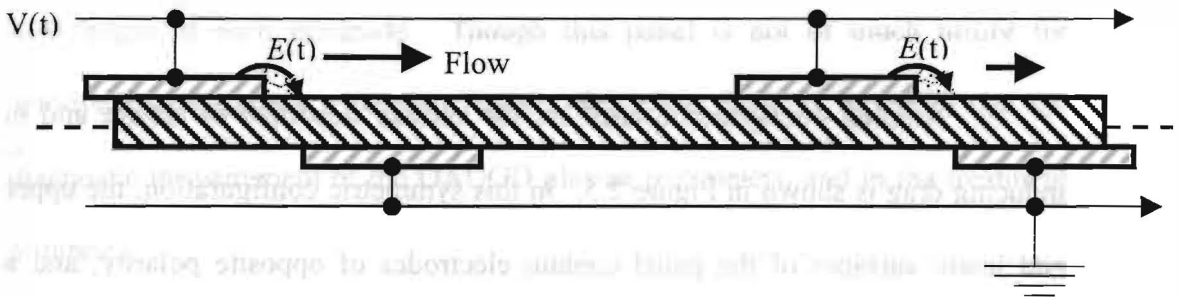





Figure 2.6 Asymmetric paraelectric panel used for flow acceleration.

-  **Metal Electrode**
-  **Dielectric**
-  **Plasma**

A layout of a pure paraelectric panel made of aluminum oxide (Al_2O_3), and its dimensions, is shown in Figure 2.7. This panel has nickel plated molybdenum electrodes of thickness 0.06 mm. These electrodes may be considered “flush” with the panel surface, as their thickness is less than the height of the maximum of the induced boundary layer flow velocity above the panel. The ceramic panel is 0.6 mm thick. As the plasma is formed above the horizontal gap between the top and bottom electrodes, it accelerates the airflow to the left.

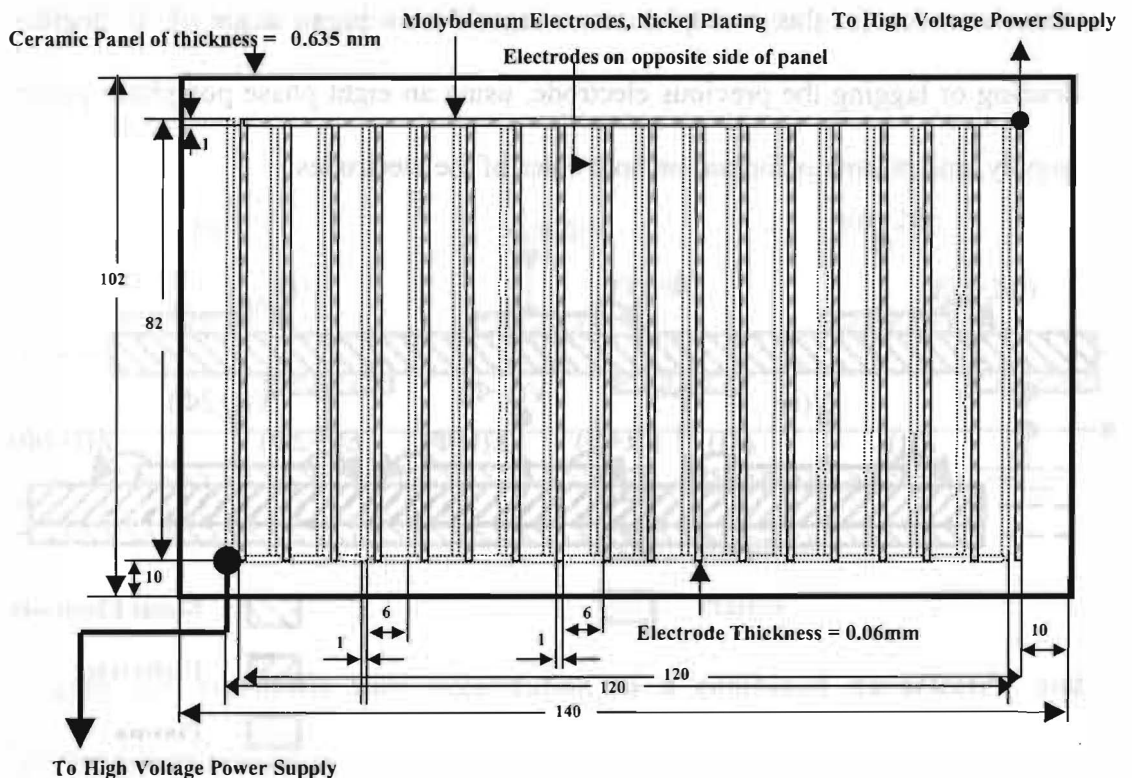


Figure 2.7 Aluminum oxide (Al_2O_3) paraelectric panel (dimensions in mm).

2.3.2 Peristaltic Plasma Actuators

Peristaltic panels differ from paraelectric panels in both the layout of electrodes and the manner in which the RF voltage is supplied to the individual electrodes. While all electrodes are energized in phase in the paraelectric mode, individual electrodes in the peristaltic mode are energized by RF voltages with different phase angles.

Peristaltic panels can be classified into two categories, namely 'pure peristaltic panels' and 'combined paraelectric and peristaltic panels'. In a pure peristaltic panel, the top of the panel contains individual strip electrodes, and the bottom surface is a solid sheet of electrical conductor. As shown in Figure 2.8, the electrodes (in this example) are energized at a phase angle of 45 degrees leading or lagging the previous electrode, using an eight phase polyphase power supply, and plasma is formed on both sides of the electrodes.

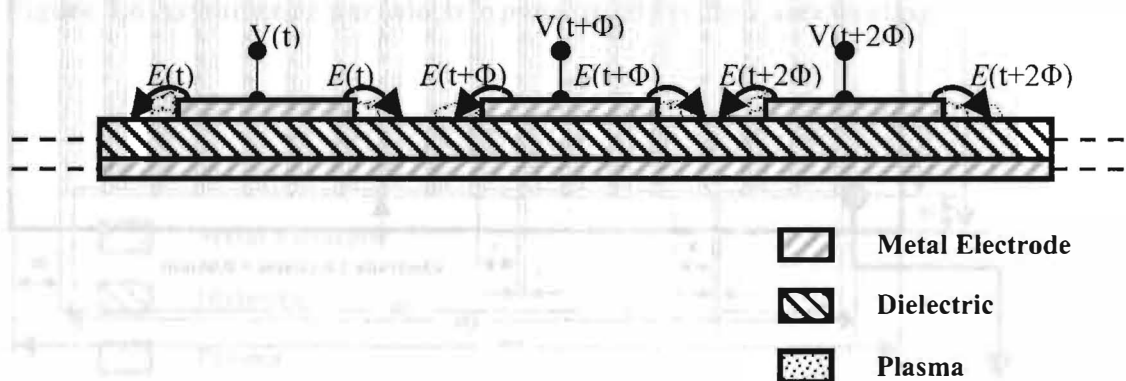


Figure 2.8 Peristaltic flow acceleration due to traveling electrostatic wave.

This excitation produces a traveling electrostatic wave that accelerates the ions. Due to Lorentzian momentum transfer by ion-neutral collisions, the neutral gas is accelerated. The paraelectric flow acceleration effects on either side of the electrodes are cancelled out by the adjacent electrode, thus leading to a purely peristaltic flow mechanism. However, the paraelectrically induced gas flows away from both sides of each electrode and creates vortices and disrupts the peristaltic flow acceleration process by generating turbulence [13].

To avoid the turbulence caused by opposing paraelectrically induced gas flows, the combined paraelectric and peristaltic actuator configuration of Figure 2.9 is used. Electrodes in this configuration are placed on both sides of the dielectric to form a paraelectric plasma actuator. All eight phases are energized

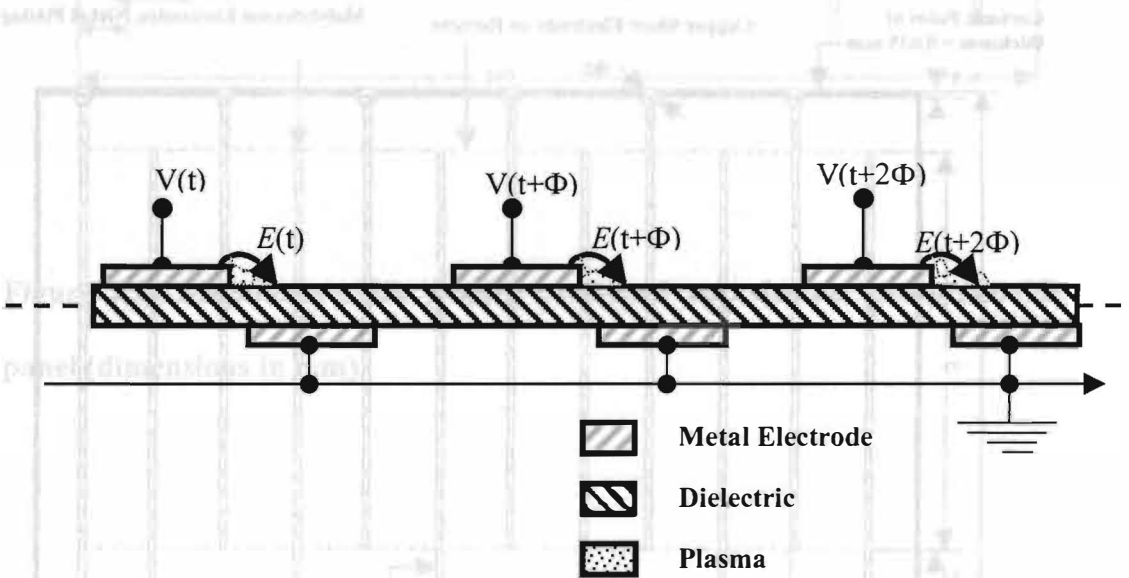


Figure 2.9 Peristaltic flow acceleration in a combined paraelectric and peristaltic acceleration.

with separate such actuators, thus avoiding turbulence caused by the upstream-induced paraelectric flow from the pure peristaltic configuration of Figure 2.8.

The configuration of Figure 2.9 adds the paraelectrically induced flow velocity from each actuator to the peristaltically induced flow velocity.

The layout and dimensions of the pure peristaltic panel and combined paraelectric and peristaltic panel are shown in Figures 2.10 and 2.11, respectively.

These panels all have nickel-plated molybdenum electrodes 0.06 mm thick. The ceramic panel is 0.635 mm thick, and the electrodes are separated by a distance of 11 mm.

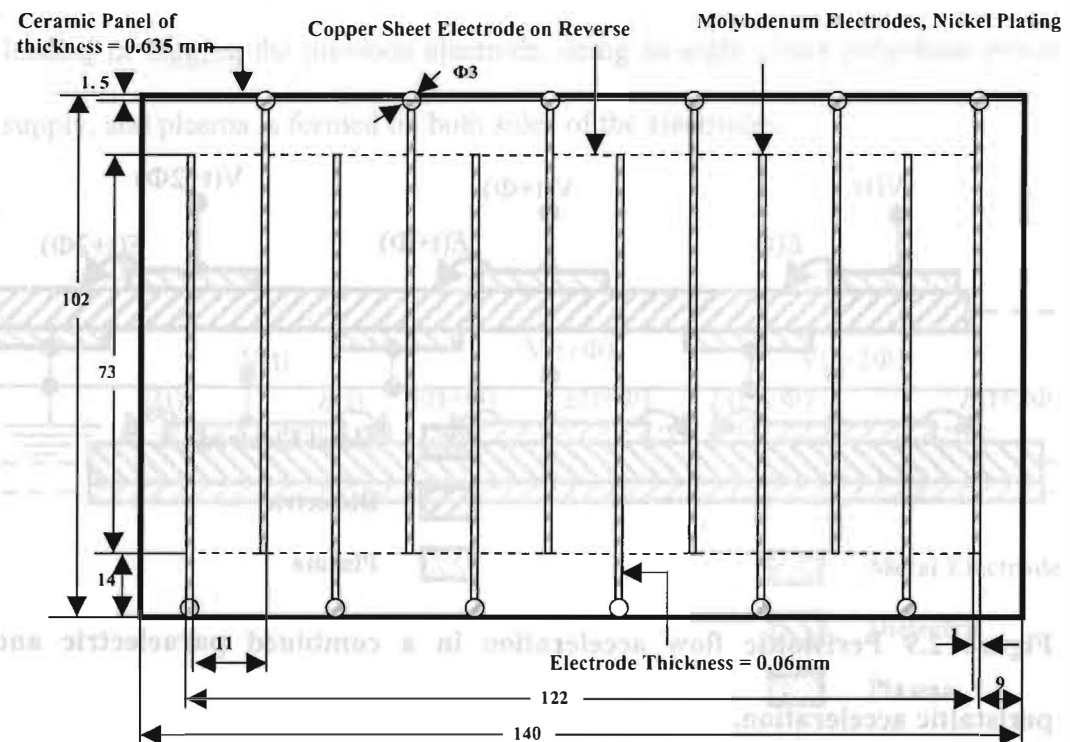


Figure 2.10 Aluminum oxide (Al_2O_3) pure peristaltic panel (dimensions in mm).

3. EXPERIMENTAL SET-UP

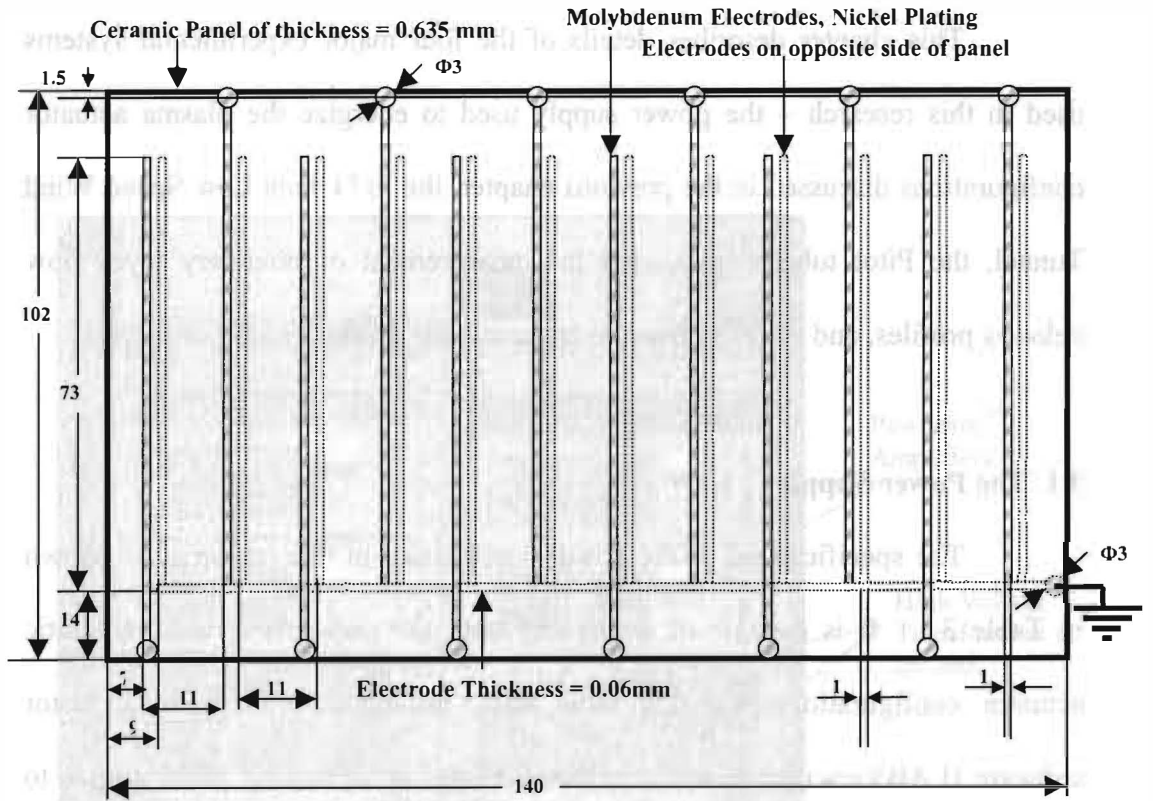


Figure 2.11 Aluminum oxide (Al_2O_3) combined paraelectric and peristaltic panel (dimensions in mm).

Table 3.1 Characteristics of the Power Supply

Manufacturer	Equipment	Model	Supply
Industrial Transformer	Transformer (4)	VT-37-KM-10P	220V AC Power
General	Frequency transformer		0.5 to 20 kHz
	Power source		0.5 to 100 W

3. EXPERIMENTAL SET-UP

This chapter describes details of the four major experimental systems used in this research – the power supply used to energize the plasma actuator configurations discussed in the previous chapter, the 7x11 Inch Low Speed Wind Tunnel, the Pitot tube system used for measurement of boundary layer flow velocity profiles, and the experimental apparatus for smoke visualization tests.

3.1 The Power Supply

The specifications of the power supply used in this research are shown in Table 3.1. It is capable of energizing both the paraelectric and peristaltic actuator configurations. For the latter case, polyphase waveform generator software (LABView) was used to obtain voltages at increasing phase angles to energize peristaltic plasma actuators. The signal generator, combined with Powertron™ amplifiers and high voltage transformers, is capable of generating RF signals with a voltage up to 10 kV_{RMS} and a frequency up to 20 kHz. Figure 3.1 shows a digital image of the power supply.

Table 3.1 Characteristics of the Power Supply

	Powertron™ Amplifiers (4)	High Voltage Transformers (4)
Manufacturer	Industrial Test Equipment Co., Inc	Industrial Test Equipment Co.,Inc
Model	1500CN AC Power Supply	VT-35/RM-109
General	Gain ≈ 110 to 130 Frequency range: 0.5 to 20 kHz	Primary/secondary turns ratio = 1:40 Center tapped secondary winding Maximum output voltage: 10 kV

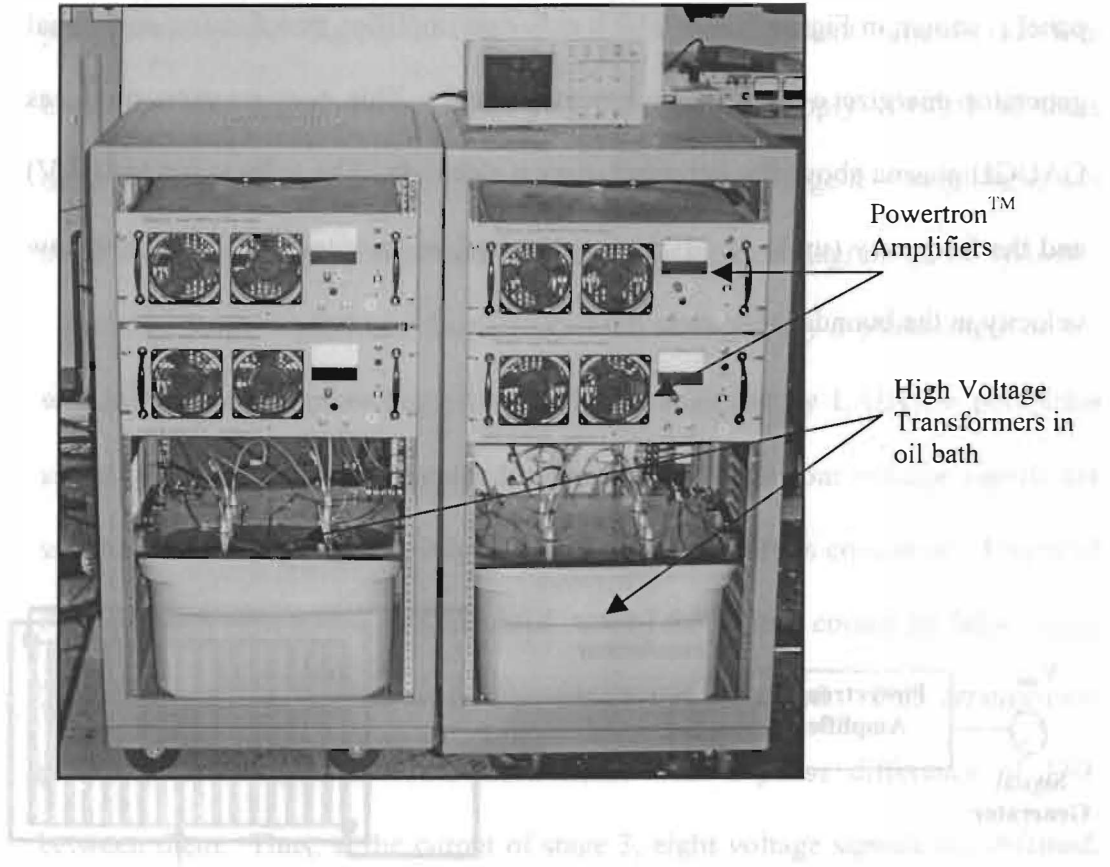


Figure 3.1 Digital image of the power supply composed of Powertron™ amplifiers (above) and high voltage transformers (below).

3.1.1 Power Supply for Paraelectric Plasma Actuators

Since all the electrodes on a paraelectric panel are energized with the same phase angle, their arrangement and connections are simpler than those of the peristaltic plasma actuators. A schematic diagram of an energized paraelectric panel is shown in Figure 3.2, in which only one amplifier, transformer, and signal generator energize a paraelectric actuator panel. This configuration produces OAUGD plasma above the flat panel at each electrode. The voltage (up to 10 kV) and the frequency (up to 12 kHz) can be optimized to obtain the maximum flow velocity in the boundary layer.

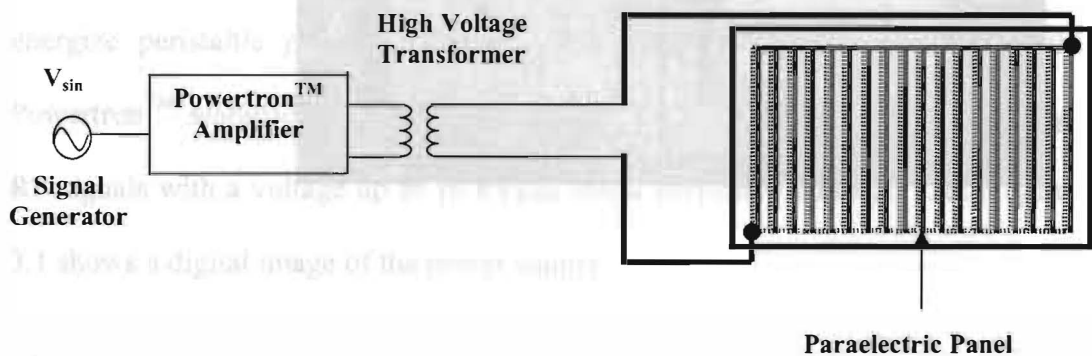


Figure 3.2 Paraelectric plasma actuator energized by the power supply.

3.1.2 Peristaltic Plasma Actuator Power Supply

The power supply for peristaltic plasma actuators is more complex than that for the paraelectric plasma actuators since it requires, in addition, a polyphase waveform generator and multiple power supplies and transformers. Unlike the paraelectric power supply of Figure 3.2, this arrangement requires all four amplifiers and transformers. The polyphase power supply consists of three different stages, Stage 1 – polyphase signal generator; stage 2 – amplifiers; and stage 3 – high voltage transformers. Figure 3.3 is a block diagram of the system.

Stage 1 produces four signals each advanced by a phase angle of 45° with respect to the preceding phase. This is achieved by LABview polyphase signal generator software described in Section 3.2. All four voltage signals are supplied to the amplifiers at Stage 2. The power amplifiers consist of 24 pairs of P-type and N-type MOSFETS mounted on a heat sink and cooled by fans. Stage 3 consists of transformers with their center tap grounded. This arrangement produces two outputs for each transformer with a phase difference of 180° between them. Thus, at the output of stage 3, eight voltage signals are obtained, each advanced by a phase difference of 45° with respect to the preceding signal. These 8 polyphase outputs provide the RF high voltage input to the actuators on the plasma panel.

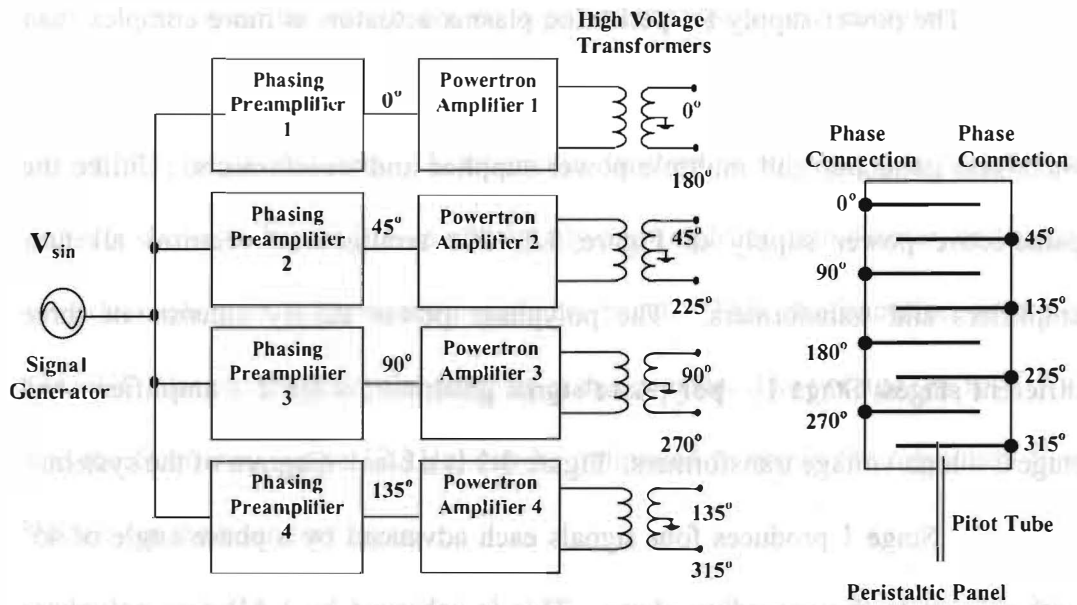


Figure 3.3 Block diagram of the power supply used to drive peristaltic plasma actuators.

3.2 Polyphase Signal Generator (LabVIEW™)

As shown in Figure 3.3, four signals, three of them advanced by a phase angle of 45° with respect to the preceding phase, are required at the output of stage 1. The polyphase signal generator software incorporated in 'LabVIEW' is employed for this purpose. This software is manufactured by National Instruments and is an open environment designed for interfacing with any measurement hardware. LabVIEW has more than 450 built-in functions designed to extract useful information from any set of acquired data, to analyze measurements, and to process signals. It also provides tools for data visualization, user interface design, Web publishing, report generation, data management, and software connectivity.

The main difference between LabVIEW and other program development environments is that, unlike the programming languages C and C++ that use codes, LabVIEW uses a graphical language 'G' to create programs in the form of block diagrams. These programs, known as virtual programs (VIs), were written using block diagrams to obtain four waveforms with a phase difference of 45° between them [14].

The LabVIEW is run using the driver software called NI-DAQ, as the latter acts an interface between the computer and the PCI 6713/AT-AO-6 analog output card. The data acquisition (DAQ) hardware is the component of the power supply system that generates the desired analog output. A schematic diagram of the driver and hardware is shown in Figure 3.4.

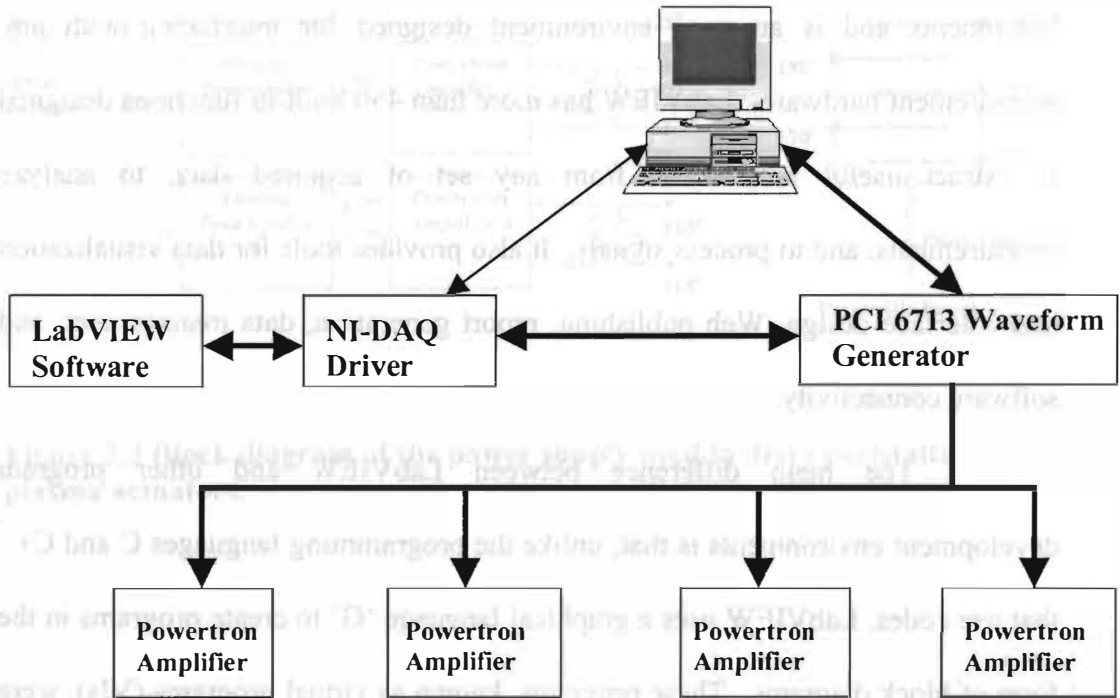


Figure 3.4 Schematic of the polyphase signal generator.

The front panel for control of the polyphase signals is shown in Figure 3.5 [15]. The amplitude of all four polyphase signals can be changed independently or collectively, depending upon requirements. The green button shown at the top-left of the panel reverses the phasing of the polyphase signals. The blue button located at the bottom is used to shutdown the whole system in emergency conditions. The offset and update rate can be changed with the help of the bars shown in Figure 3.5. The update rate is changed in order to change the frequency of operation.

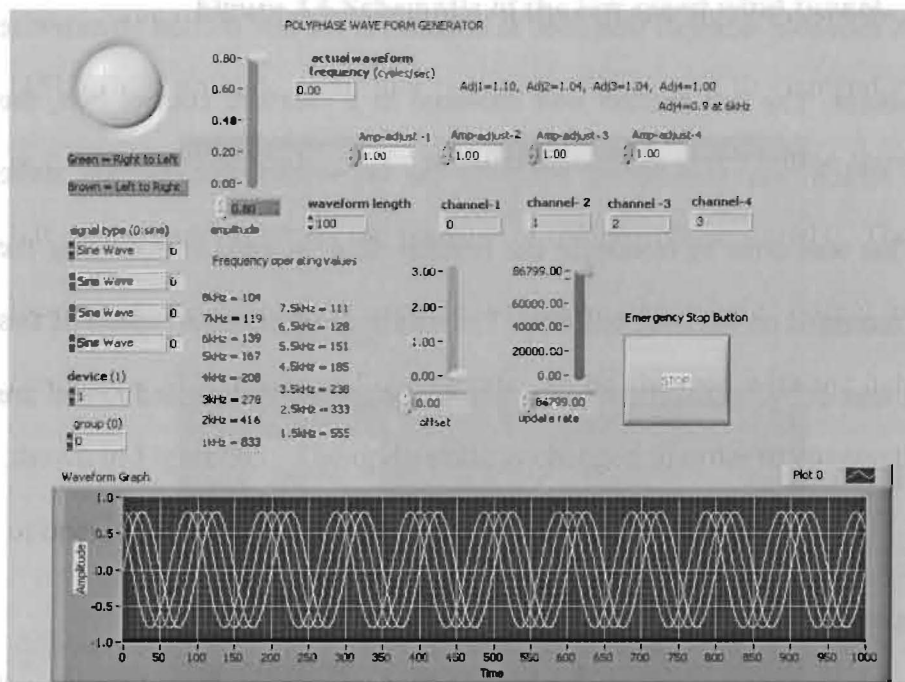


Figure 3.5 Front panel of the LabVIEW polyphase generator program.

3.3 The Wind Tunnel

Both the boundary layer velocity profiles and smoke flow visualization tests were run in the 7 x 11 Inch (18 x 28 cm) Low Speed Wind Tunnel at the NASA Langley Research Center, Hampton, VA. The tunnel is a conventional, straight-through, open-return configuration powered by a variable-pitch, multi-blade axial fan located at the exit, providing a precisely controlled airspeed in the test section. The wind tunnel has a test section with dimensions 178 mm high x 279 mm wide x 914 mm long. The panels under test were mounted on a drag balance occupying a 305 mm wide x 279 mm long central region of the bottom test section wall.

A movable sidewall was used to counteract the test section streamwise pressure gradient. The test section was enclosed in a pressure control box, the pressure of which was maintained equal to the freestream test section static pressure. This was done to minimize the leakage flow in gaps surrounding the panel when mounted on the drag balance. The maximum freestream speed of this wind tunnel was 26 m/s. A schematic and a digital image of the wind tunnel are shown in Figures 3.6 and 3.7 respectively.

3.4 Pitot Tube System

A Pitot tube system, shown schematically in Figure 3.8, was employed to measure the boundary layer velocity profile. The Pitot pressure for boundary layer profiles was measured with a quartz electronic pressure transducer

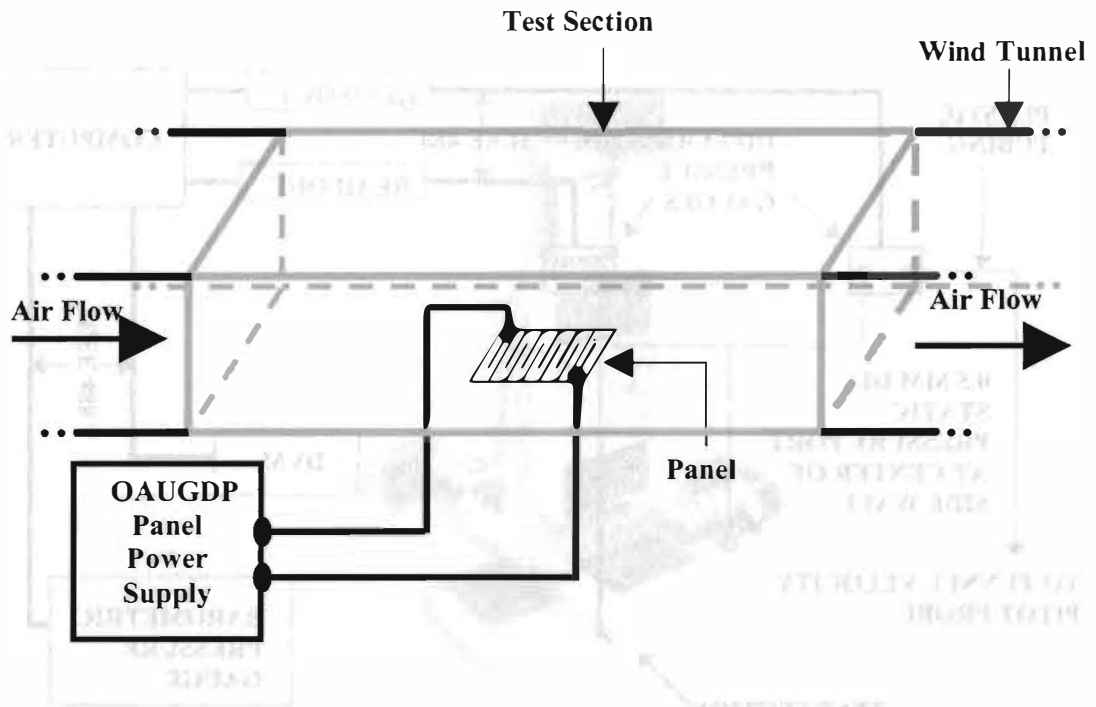
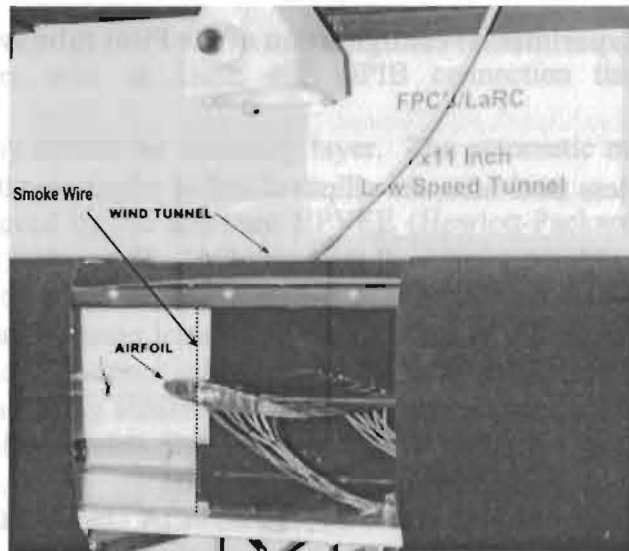


Figure 3.6 Schematic of the low speed wind tunnel.



3.7 Digital image of the NACA 0015 airfoil with OAUGDP electrode strips mounted in the NASA Langley Research Center's 7 X 11 Inch Low Speed Wind Tunnel.

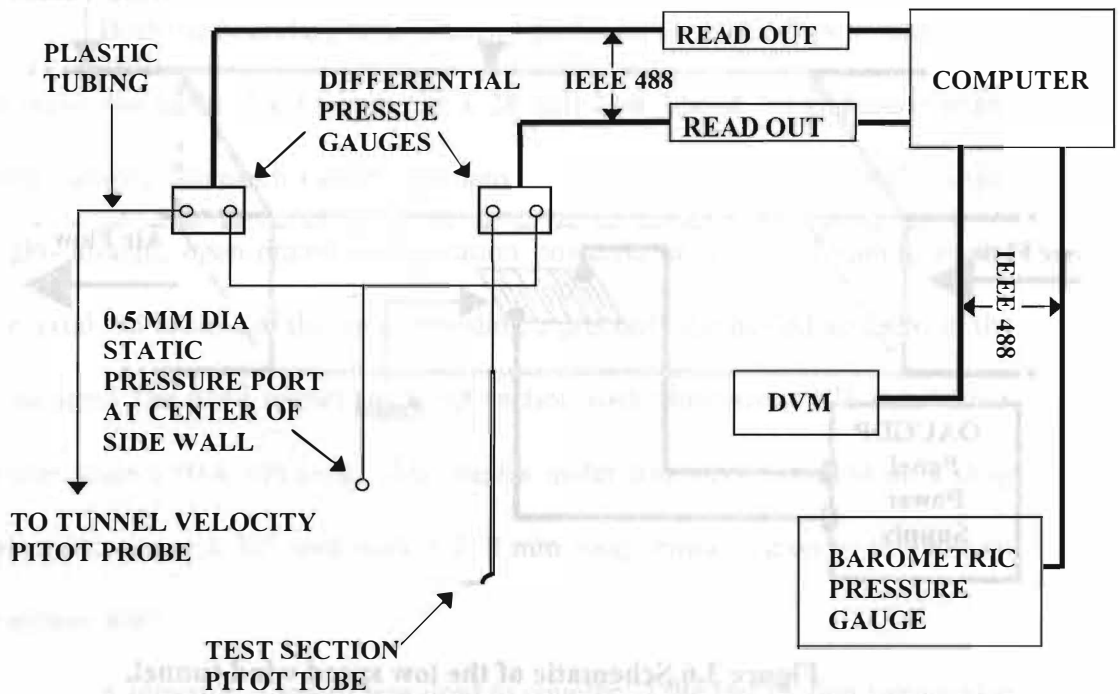


Figure 3.8 Experimental configuration of the Pitot tube system.

connected to a stainless steel tube, the elliptical end of which was 0.28 mm high and 0.65 mm wide, with a 0.1 mm wall thickness [16]. The system also included 2 differential pressure gauges to measure the differential pressure inside the wind tunnel, and a barometric pressure gauge. All three pressure gauges are connected to the computer through an IEEE 488 GPIB connection.

A commercially available traversing mechanism made by Aerotech and shown in Figure 3.9 was used to move the Pitot tube in three dimensions at speeds up to 100 mm/s. It consists of a digital step motor controller connected to



Figure 3.9 Pitot tube positioner AT5100 series.

the computer with an IEEE 488 GPIB connection that moves the probe automatically across the boundary layer. The automatic movement of the Pitot tube is achieved by the software HPVEE (Hewlett-Packard Visual Engineering Environment), which is programmable in a graphic environment. The parameters of each run can be specified by setting the number of measurements to be taken, the length of each step, the total distance to be moved, and the number of data points to be averaged. After the run, HPVEE stores the data obtained in text (.txt) format, which can be plotted later for graphical presentation. The overall system is shown in the next chapter.

3.5 Smoke Wire Flow Visualization System

A smoke wire flow visualization system was employed to study turbulence in the boundary layer. A block diagram of the essential components of this system is shown in Figure 3.10. A 0.1 mm diameter stainless steel wire is placed vertically 15 mm upstream from the edge of the first electrode on the plasma panel. A small weight was tied to the bottom end of the wire to hold it taut. For every run, the wire was coated with mineral oil in such a way that the oil, because of its surface tension, would form small, approximately equally spaced droplets along the length of the wire. The smoke wire was Joule heated by current from a DC power supply. When the triggering unit heats the smoke wire with a current pulse, the beads of mineral oil are vaporized, thus forming smoke trails in the wind tunnel flow. The flow visualization photography was done with a digital, progressive-scan, monochromatic video camera with 768 x 484 pixel sensing elements and a 3.5-4.5, 75-200 mm zoom lens [16].

The time delay unit plays a crucial role in this system. While triggering both the smoke wire firing system and the strobe system, it creates a delay of a few ms between the time the wire is energized and the time when the smoke trails are illuminated by the strobe light. The delay is adjusted to capture the image of smoke trails traveling over the top of the panel placed in the test section. The experimental arrangement of the overall system is shown in the next chapter.

4. EXPERIMENTAL RESULTS

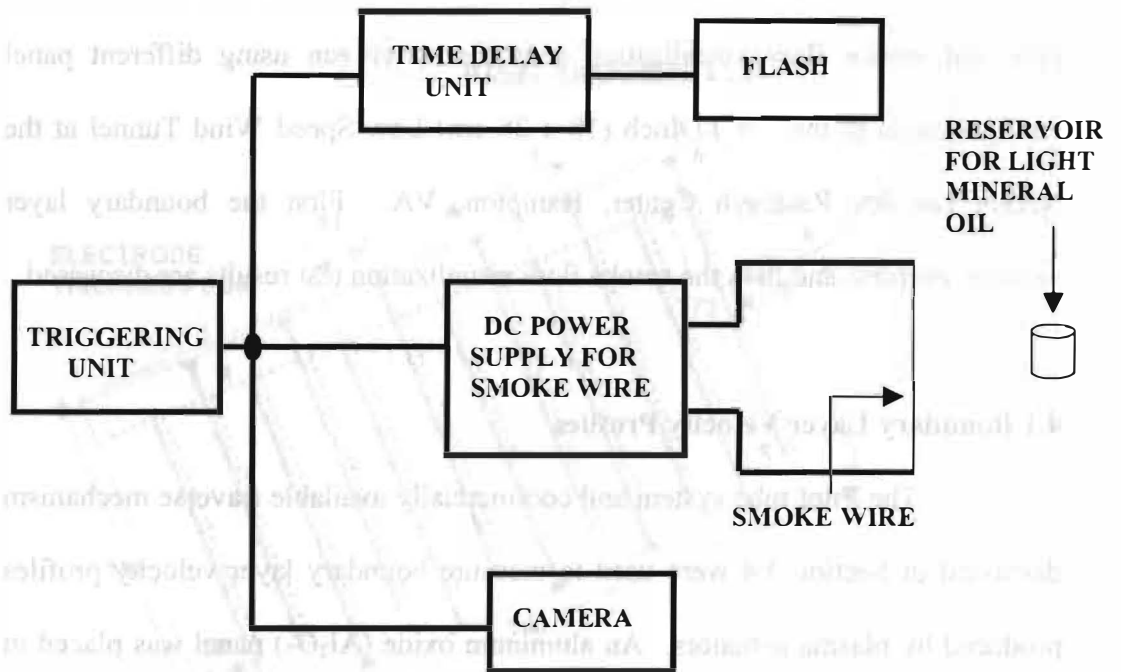


Figure 3.10 Components of the smoke wire flow visualization system.

4. EXPERIMENTAL RESULTS

This chapter describes experimental results obtained from the Pitot tube and smoke flow visualization tests that were run using different panel configurations in the 7 x 11 Inch (18 x 28 cm) Low Speed Wind Tunnel at the NASA Langley Research Center, Hampton, VA. First the boundary layer velocity profiles, and then the smoke flow visualization test results are discussed.

4.1 Boundary Layer Velocity Profiles

The Pitot tube system and commercially available traverse mechanism discussed in Section 3.4 were used to measure boundary layer velocity profiles produced by plasma actuators. An aluminum oxide (Al_2O_3) panel was placed in the test section of the wind tunnel. The tip of the Pitot tube was mounted at a horizontal distance 15 mm downstream from the edge of the last electrode on the panel. Figures 4.1 and 4.2 show the Pitot tube over the panel, and a digital image of the placement of the Pitot tube, respectively. The Pitot tube was circular, with outer and inner diameters of 0.5 mm and 0.36 mm, respectively, as shown in Figure 4.3. During measurements, the Pitot tube was moved laterally over the width of the panel in the horizontal direction and as much as 3 cm above the surface of the panel in the vertical direction. An adequate distance between the tip of the Pitot tube and the electrodes was maintained to avoid sparking. This is why the boundary layer profile along the flow direction was not taken. A schematic of the system is shown in Figure 4.4.

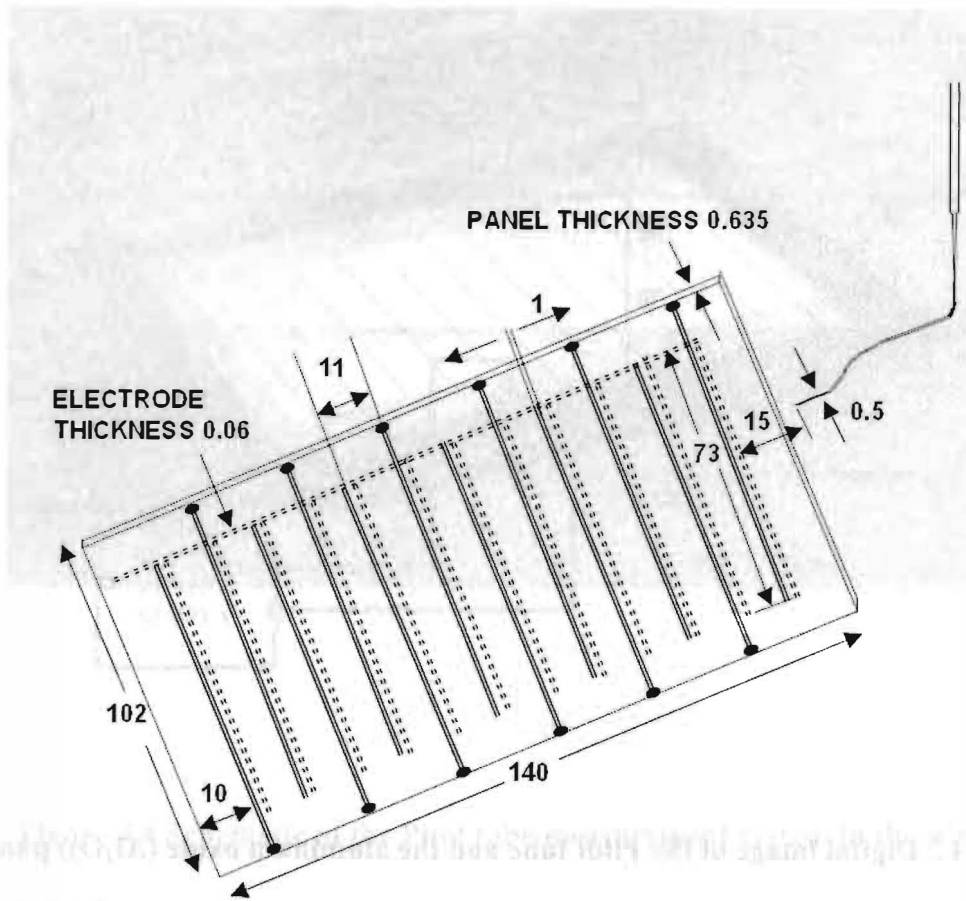


Figure 4.1 Schematic drawing of an aluminum oxide panel, showing the position of the Pitot tube above the panel.



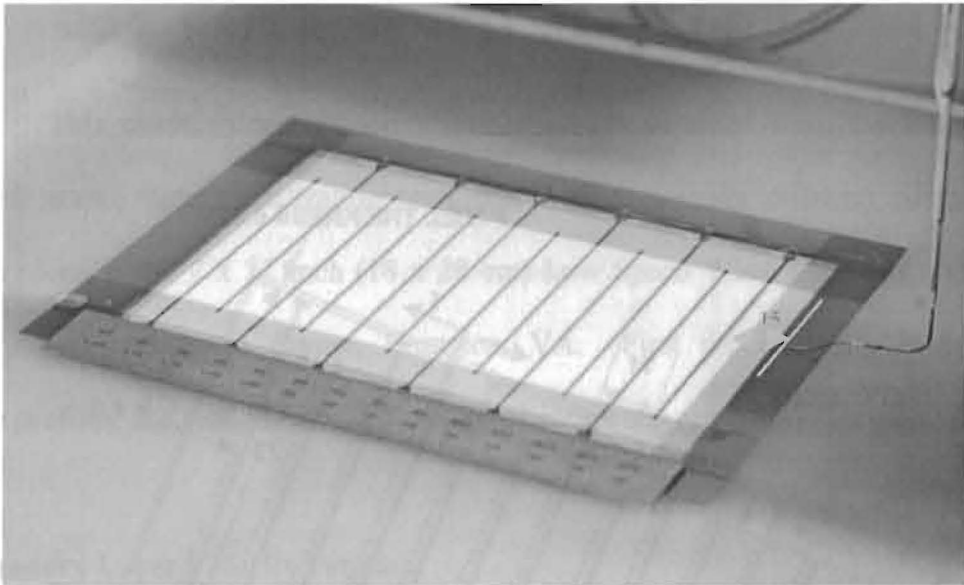


Figure 4.2 Digital image of the Pitot tube and the aluminum oxide (Al_2O_3) panel mounted in the wind tunnel.

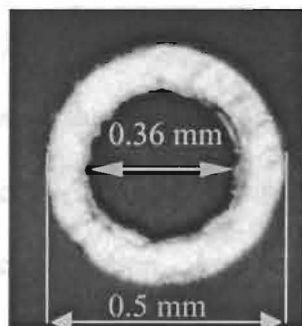


Figure 4.3 Digital image of the opening of the Pitot tube.

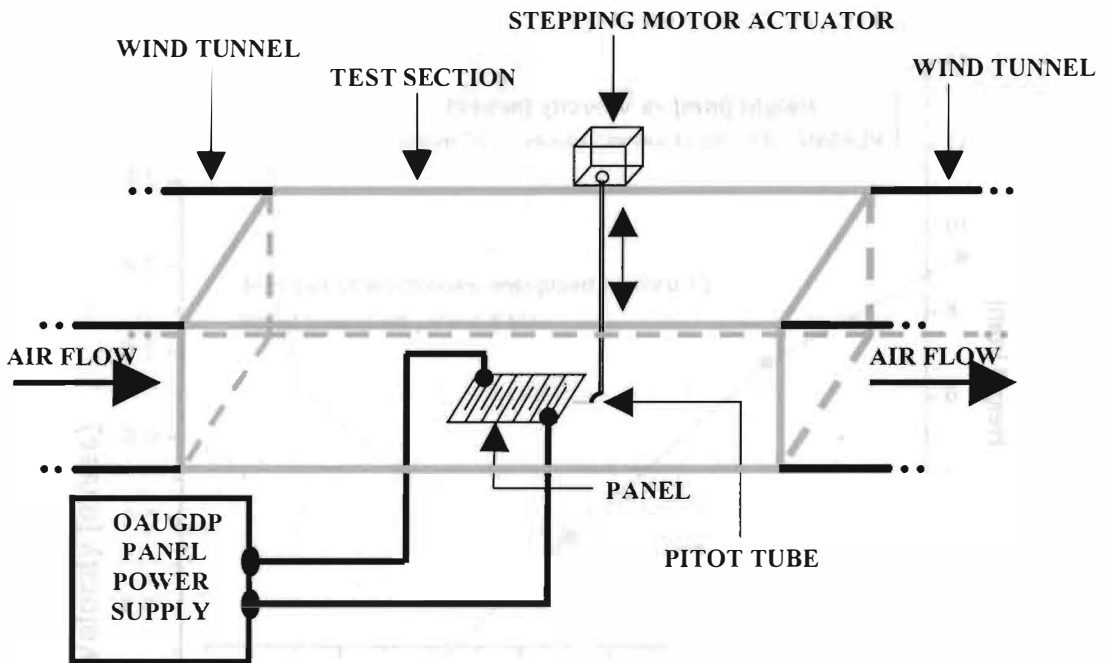


Figure 4.4 Schematic of the Pitot tube measurement system in the wind tunnel.

4.2 Boundary Layer Profile with Plasma Off

The combined paraelectric and peristaltic plasma actuator panel shown in Figure 2.9 was run in the pure paraelectric mode. A positive velocity offset of 0.5 m/sec was introduced by the Pitot tube measuring system. Vertical profiles were taken up to a height of 12 cm. A boundary layer velocity profile with a wind tunnel free-stream velocity of 3.95 m/sec is shown in Figure 4.5 when none of the plasma actuators were energized [17].

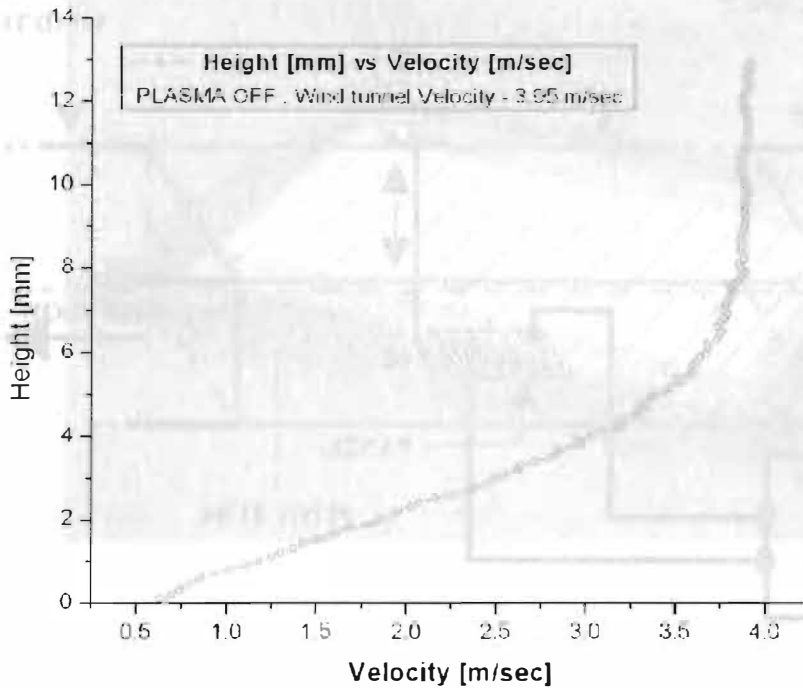


Figure 4.5 Velocity profile with plasma off and wind tunnel free stream velocity of 3.95 m/sec.

4.3 Effect of Frequency

To determine the effect of RF frequency on flow velocity, several tests were run with all 12 plasma actuators on the panel energized at a constant voltage of 4.5 kV. In these tests, the wind tunnel was turned off in order to measure the velocity induced solely by the actuators. As illustrated in Figure 4.6, the velocity increased linearly with the applied RF frequency. A reason that may account for this phenomenon is that more and more ions are trapped with the increasing applied RF frequency, thus increasing the plasma density.

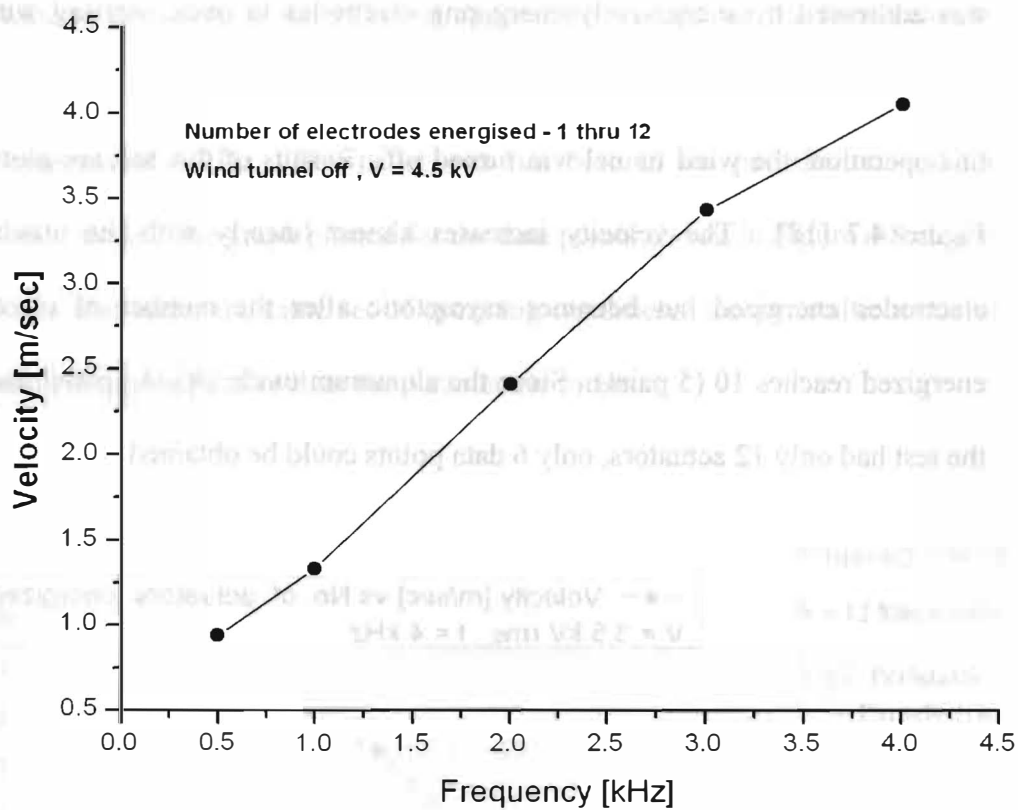


Figure 4.6 Flow velocity plotted as a function of applied RF frequency.

4.4 Effect of Number of Electrodes Energized

The effect of the number of electrodes energized on the flow velocity was addressed by successively energizing electrodes in pairs, starting with the electrodes closest to the Pitot tube, until all 12 electrodes were energized. During this operation, the wind tunnel was turned off. Results of this test are plotted in Figure 4.7 [18]. The velocity increases almost linearly with the number of electrodes energized but becomes asymptotic after the number of electrodes energized reaches 10 (5 pairs). Since the aluminum oxide (Al_2O_3) panel used for the test had only 12 actuators, only 6 data points could be obtained.

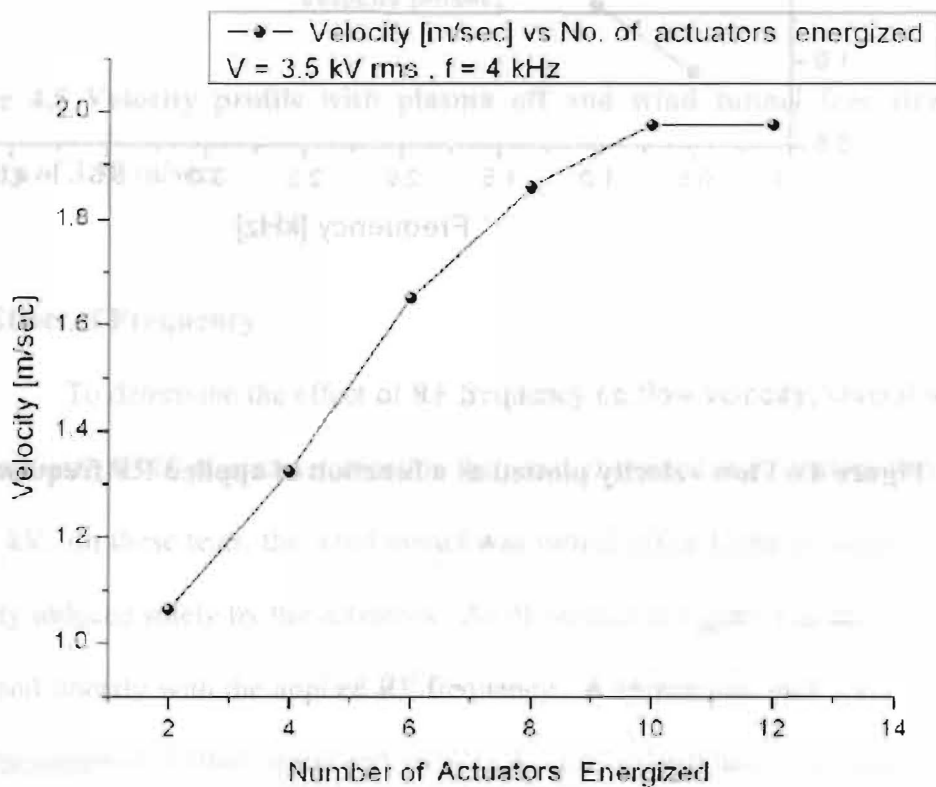


Figure 4.7 Flow velocity plotted as a function of number of electrodes energized.

4.5 Effect of Applied RF Voltage

The combined piezoelectric and peristaltic panel shown in Figure 2.9 was used to demonstrate the effect of applied RF voltage on the flow velocity. For this test, all 12 actuators on the panel were energized, and the frequency was kept constant at 6 kHz. The panel was run both in the piezoelectric and the peristaltic mode. The graph plotted for the data points shown in Figure 4.8 clearly illustrates that under the same set of operating conditions, the peristaltic mode of operation is more effective than the piezoelectric mode.

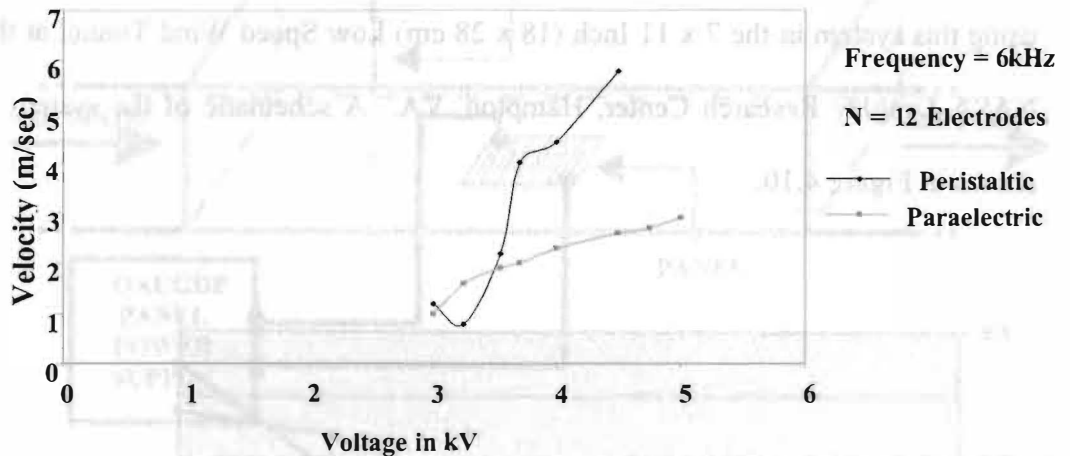


Figure 4.8 Effect of voltage and the mode of EHD operation on the flow velocities.

Experiments were also conducted in order to demonstrate the effect of applied voltage at different frequencies on the flow velocity. The panel was run in the pure peristaltic mode, and the voltage increased up to 3.5 kV at frequencies ranging from 1 kHz to 5 kHz. The resulting data points are plotted in Figure 4.9.

4.6 Smoke Flow Visualization Tests

The smoke flow visualization system discussed in Section 3.5 was employed to study the effect of plasma actuators on the flow in the boundary layer. The three panel configurations shown in Figures 2.7, 2.10, and 2.11 were tested using this system in the 7 x 11 Inch (18 x 28 cm) Low Speed Wind Tunnel at the NASA Langley Research Center, Hampton, VA. A schematic of the system is shown in Figure 4.10.

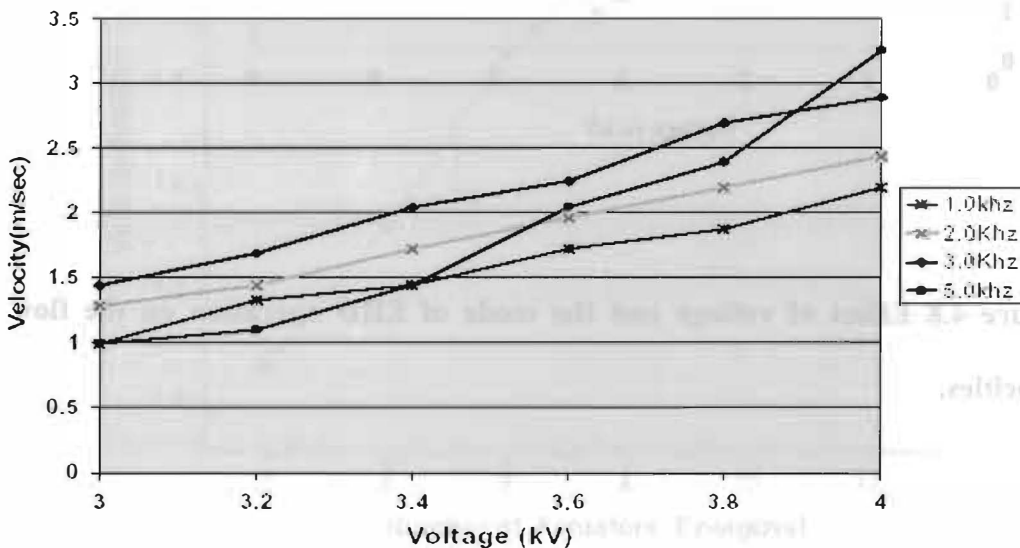


Figure 4.9 Effect of applied RF voltage and frequency on the flow velocities.

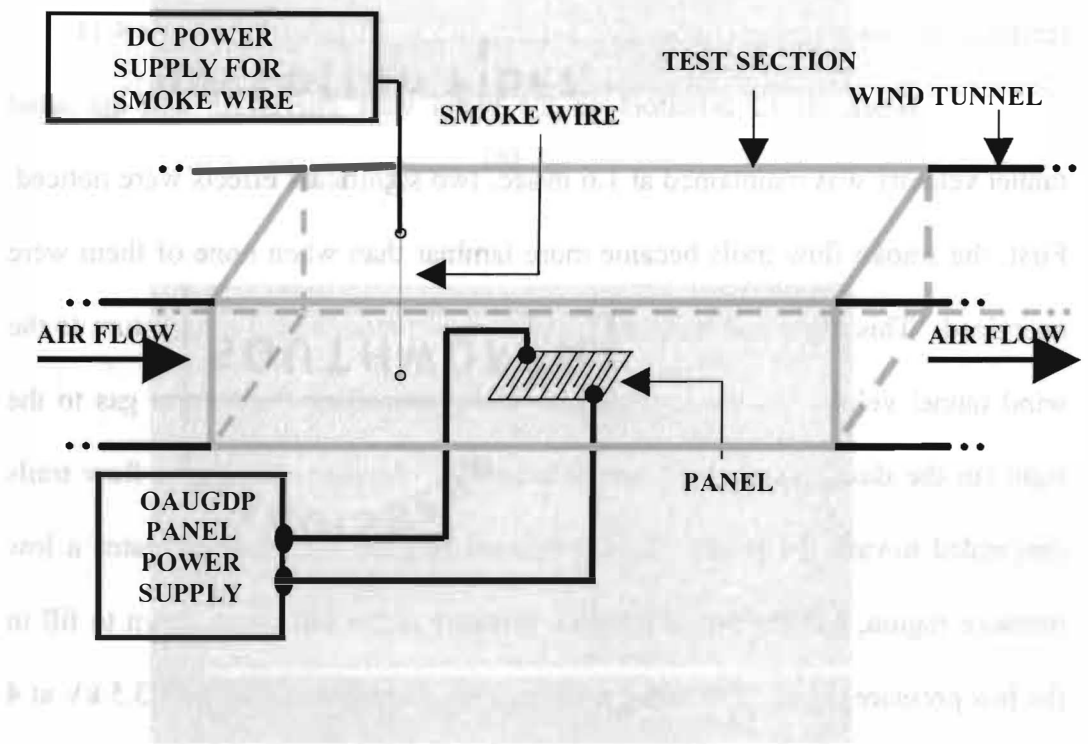


Figure 4.10 Experimental set-up for smoke flow visualization tests.

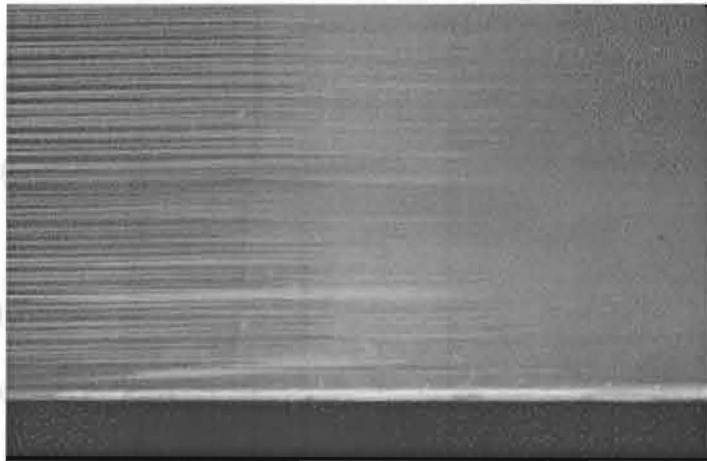
4.6.1 Smoke Flow Visualization using a Paraelectric Panel

Tests were run for the paraelectric panel with the wind tunnel velocity kept constant at 1.6 m/sec, and with the panel both energized and unenergized to demonstrate the effect of paraelectric actuators on the boundary layer flow. When the panel was unenergized, the smoke flow trails above the panel surface were generally laminar in the direction of the wind tunnel velocity, with a slight tendency to flow tripping (turbulence generation) as illustrated in Figure 4.11a.

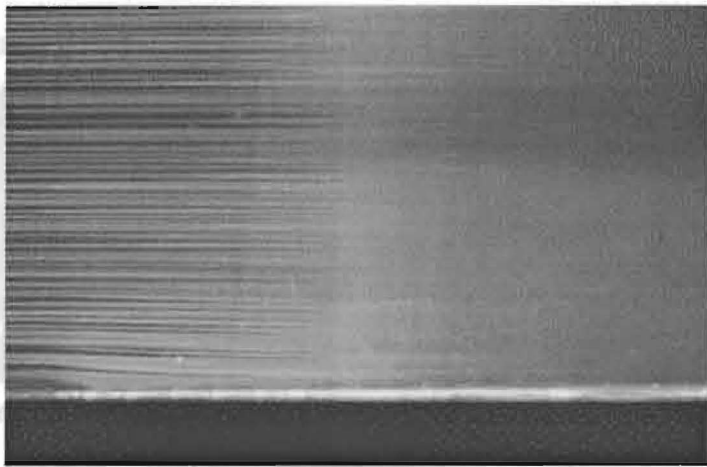
When all 12 actuators on the panel were energized, and the wind tunnel velocity was maintained at 1.6 m/sec, two significant effects were noticed. First, the smoke flow trails became more laminar than when none of them were energized. This happened because the plasma actuators added momentum to the wind tunnel velocity at the boundary layer by propelling the neutral gas to the right (in the direction of wind tunnel velocity). Second, the smoke flow trails descended toward the panel. This happened because the plasma creates a low pressure region, and the air, at a higher pressure at the top, came down to fill in the low pressure region. For these runs, actuators were energized with 3.5 kV at 4 kHz. These effects are illustrated in Figure 4.11b [19].

4.6.2 Smoke Flow Visualization using a Peristaltic Panel

Several tests were run to demonstrate the effects of pure peristaltic and combined paraelectric and peristaltic actuators on the boundary layer. The aluminum oxide (Al_2O_3) panels shown in Figures 2.10 and 2.11 were used for this



(a)



(b)

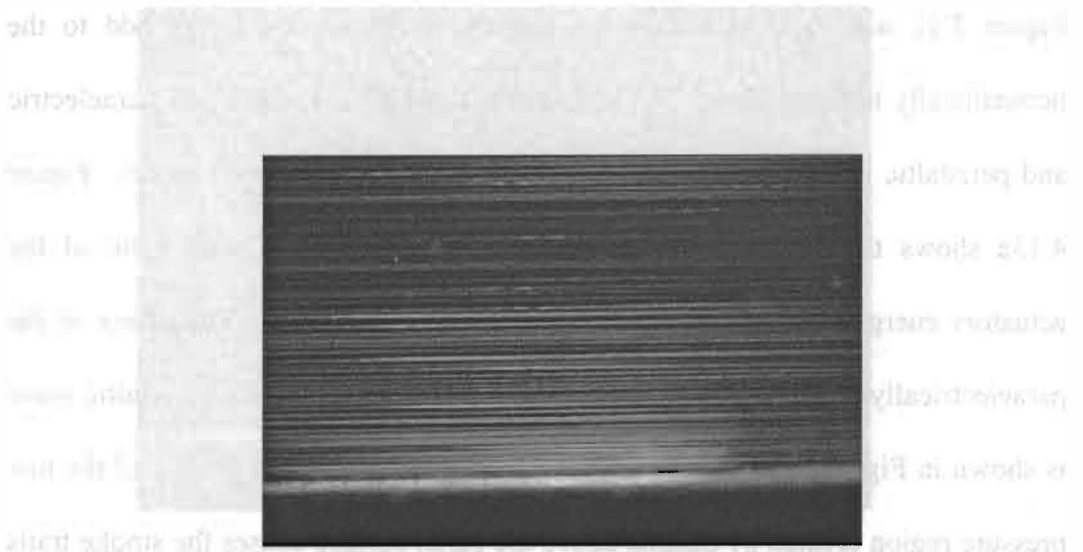
Figure 4.11 Smoke flow visualization tests for paraelectric panel. (a) Smoke flow trails with panel not energized and wind tunnel velocity of 1.6 m/sec. (b) Smoke flow trails with panel energized at 3.5 kV and 4 kHz, with a wind tunnel velocity of 1.6 m/sec.

purpose. Smoke flow trails over the panel surface at a wind tunnel velocity of 3.95 m/sec with none of the actuators energized are shown in Figure 4.12a. In this case, airflow over the panel surface is laminar.

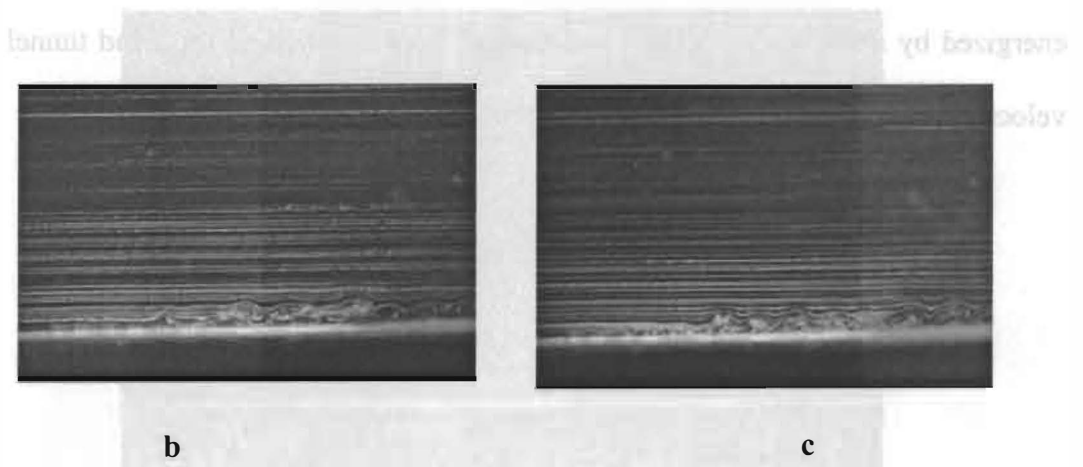
With the polyphase power supply, it was possible to reverse the direction of the induced peristaltic gas flow. The peristaltic panel shown in Figure 2.8 was energized with 3 kV and 4 kHz to document the effect of reversing the gas flow direction on the smoke flow trails. Figure 4.12b shows the effect on the smoke flow trails when all 12 actuators on the panel surface were energized, and the direction of the induced peristaltic gas flow is to the right i.e. adding momentum to the boundary layer flow. Since this panel generates plasma on both sides of each electrode, it leads to a low pressure region which forms turbulent vortices between each pair of actuators. Figure 4.12c shows the effect on the smoke flow trails when the direction of the induced peristaltic gas flow is to the left, i.e. causing negative momentum that opposes the flow. In such a case the negative flow leads to a thickened boundary layer as it mixes with the boundary layer flow. The reason for the turbulence visible in Figures 4.12b and 4.12c is that the actuator plasma creates a low pressure region on either side of the electrodes, and when the air flows downward, it is pumped to left or right depending upon the phase sequence of the polyphase power supply.

A pure peristaltic panel configuration has the disadvantage of paraelectrically induced flow counteracting the flow generated by peristaltic waves, illustrated in Figure 4.12b, and thus leading to turbulence in the boundary layer.

The combined gas turbine and peristaltic pump configuration shown in



a



b

c

Figure 4.12 Smoke flow visualization tests for pure peristaltic panel. (a) Smoke flow trails with panel not energized and wind tunnel velocity of 3.95 m/sec. (b) Smoke flow trails during positive flow with panel energized with 3 kV and 4 kHz, and wind tunnel velocity of 3.95 m/sec. (c) Smoke flow trails during negative flow with panel energized with 3 kV and 4 kHz, and wind tunnel velocity of 3.95 m/sec.

The combined piezoelectric and peristaltic panel configuration shown in Figure 2.11 was used to induce the piezoelectric flow velocity to add to the peristaltically induced flow. To demonstrate this effect, a combined piezoelectric and peristaltic panel was mounted in the test section of the wind tunnel. Figure 4.13a shows the smoke flow trails over the panel surface with none of the actuators energized at a wind tunnel velocity of 3.95 m/sec. The effect of the piezoelectrically induced flow being added to the flow induced by peristaltic wave is shown in Figure 4.13b, for which all 12 actuators were energized, and the low pressure region created by plasma above the panel surface causes the smoke trails to move downwards without generating turbulence. Actuators in this case were energized by a voltage of 3.5 kV and frequency of 4 kHz, and the wind tunnel velocity was 3.95 m/sec.

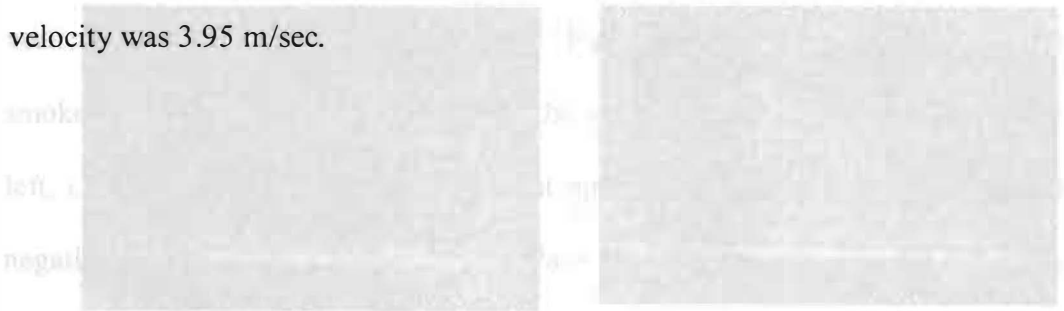
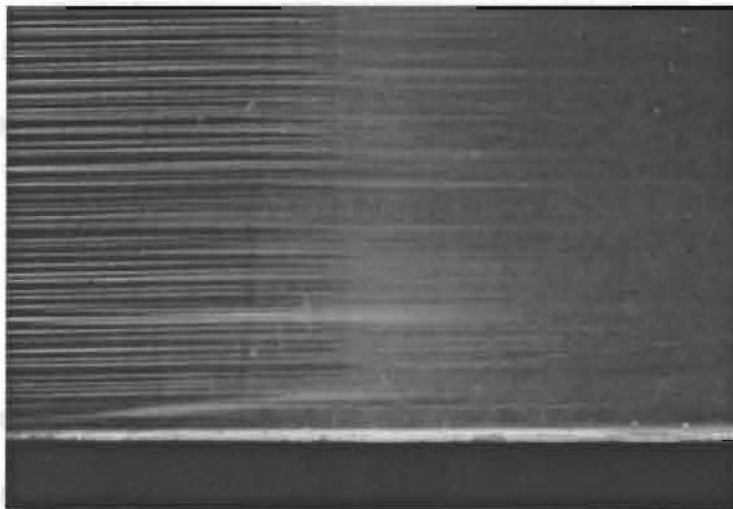
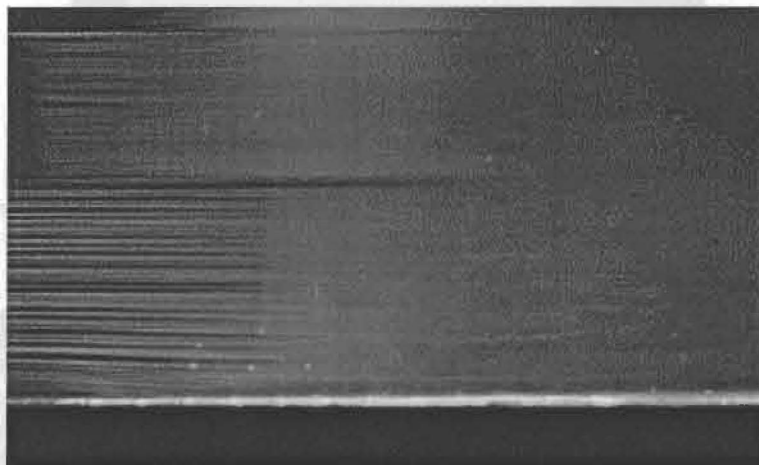


Figure 4.13 (a) Smoke flow trails over the panel surface for pure peristaltic panel. (b) Smoke flow trails over the panel surface with piezoelectrically induced flow added to the peristaltically induced flow.

Figure 4.13 shows smoke flow trails over the panel surface for pure peristaltic panel. (a) Smoke flow trails over the panel surface with piezoelectrically induced flow added to the peristaltically induced flow. (b) Smoke flow trails over the panel surface with piezoelectrically induced flow added to the peristaltically induced flow. The smoke flow trails in (a) are horizontal, while in (b) they are curved downwards. This indicates that the piezoelectrically induced flow is adding to the peristaltically induced flow, causing the smoke trails to move downwards without generating turbulence.



a



b

Figure 4.13 Smoke flow visualization tests for combined piezoelectric and peristaltic panel. (a) Smoke flow trails with panel not energized and wind tunnel velocity of 3.95 m/sec. (b) Smoke flow trails during positive flow with panel energized with 3.5 kV and 4 kHz, and wind tunnel velocity of 3.95 m/sec.

5. LOW COST POWER SUPPLY

In order to generate the OAUGDP[®] on plasma actuators at the least expense, a power supply using low cost components was developed at the UT Plasma Sciences Laboratory, and is discussed in detail in this Section.

5.1 Components of the Low Cost Power Supply

This power supply consists of three major sets of components: automotive ignition coils, audio amplifiers, and a DC battery. Each of the components and the experimental set-up are discussed in detail in the following sections.

5.1.1 Audio Amplifiers

Three hundred watt audio amplifiers, available off the shelf, were used to amplify the voltage input from a signal generator. Each amplifier is 18.4 cm long x 28.6 cm wide x 5.73 cm high. Digital images of the top and side of this amplifier are shown in Figures 5.1a and 5.1b.

Four sets of audio amplifiers provided the eight amplified outputs needed to generate OAUGDP[®] on the actuators. The audio amplifiers consist of MOSFETS mounted on a die-cast aluminum heat sink. Pulse width modulation (PWM) circuitry is used inside each amplifier to minimize electrical losses, thus, making them ecologically beneficial with significant reduction of power consumption. A typical audio amplifier of this category costs about \$75. The features of the amplifiers used in this research are shown in Table 5.1 [20].



a



b

Figure 5.1 SPL CRM300-2 audio amplifier. (a) Top view. (b) Side view.

Figure 5.2 Rotameter ignition coils. (a) Air ignition coil transformer (b)

Set of right ignition coil transformers to energize plasma solenoids

Table 5.1: Features of audio amplifiers.

S. No.	Specification
1.	Variable Low Pass 40Hz-120Hz
2.	Variable Hi Pass 150Hz-1.5Khz
3.	Frequency Response: 10Hz to 30Khz
4.	S/N Ratio: 97 dB
5.	Total Harmonic Distortion: 0.02%
6.	Full Mosfet Power Supply
7.	PWM Circuitry
8.	System Distress Indicator
9.	High/Low Level Inputs / Floating Ground
10.	Three Way Protection Circuit
11.	Full Selectable Crossover Hi / Full / Low

5.1.2 Automotive Ignition Coils

A digital image of an ignition coil used for the power supply is shown in Figure 5.2a. Automotive ignition coils were employed to function as high voltage transformers to step up the output voltage from the audio amplifiers. Like the audio amplifiers, these ignition coil transformers are also available off-the-shelf at any general auto-parts shop. A set of eight automotive ignition coils, shown in Figure 5.2b, was used to amplify the dual outputs from the four amplifiers. To minimize the design complexity, automotive ignition coils with internal resistors were used. A typical automotive ignition coil of this type costs about \$25.

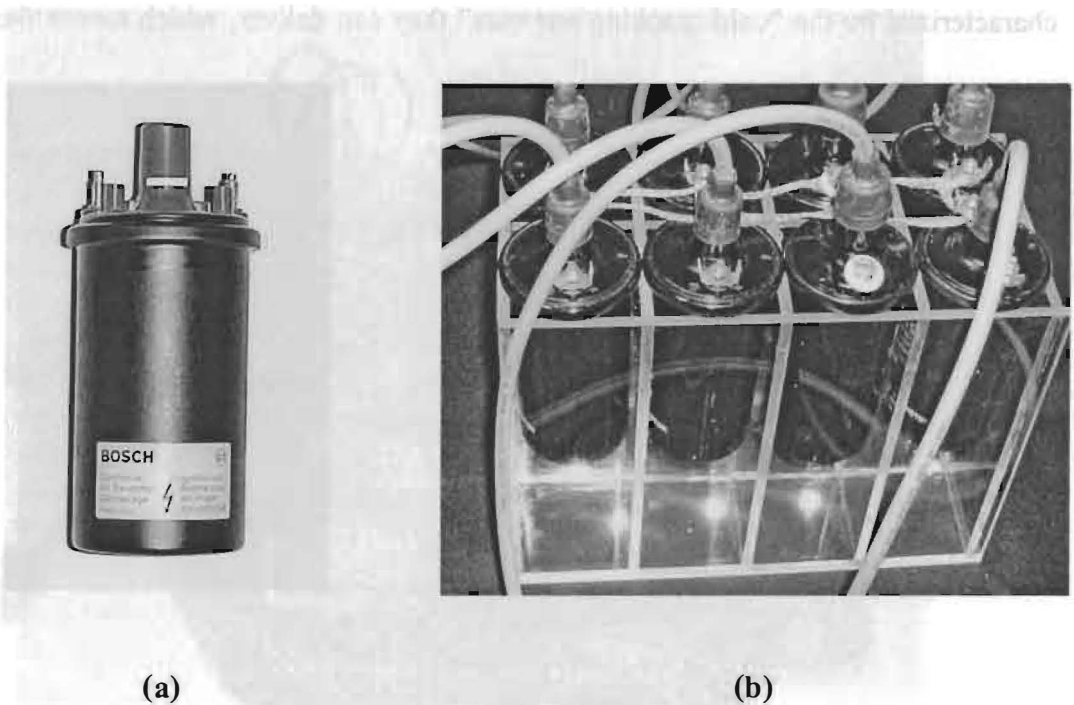


Figure 5.2 Automotive ignition coils. (a) An ignition coil transformer. (b) Set of eight ignition coil transformers to energize plasma actuators.

These automotive ignition coils have a primary/secondary turns ratio of 1:100. The primary and secondary resistance is 3.9 ohms and 7 ohms respectively. The resistance of the wire used to connect the output terminal of the ignition coils to the actuators is 6.7 ohms. The output voltage waveforms of the ignition coils were measured to confirm that all the ignition coils delivered the same output voltage at the same operating conditions.

5.1.3 DC Battery

The 12 volt DC battery shown in Figure 5.3, commonly used in automobiles, was used to drive the audio amplifiers. These batteries are characterized by the “cold cranking amperes” they can deliver, which means the



Figure 5.3 12V DC battery.

discharge load measured in amperes that a fully charged battery at 0 degrees F (-17.8 degrees C) can deliver for 30 seconds while maintaining the voltage above 7.2 volts. The cold cranking value for the battery used in these experiments was 650 amperes, while its cold cranking value at 32⁰ F (0⁰ C) was 780 amperes. A typical battery costs about \$90.

A major problem encountered during our experimental program was that the battery would discharge after a few runs. Thus, a battery charger, shown in Figure 5.4, was used that takes about an hour to fully charge the battery. A typical battery charger costs about \$40.



Figure 5.4 Battery charger.

5.2 Experimental Set-up

A schematic of the polyphase power supply is shown in Figure 5.5. The power supply consists of four audio amplifiers and eight automotive ignition coil transformers. The signal generator, audio amplifiers and automotive ignition coils, are capable of generating an eight phase polyphase RF signal with voltages up to 7 kV and frequencies up to 8 kHz. The power supply consists of three stages; Stage 1 – signal generator and DC battery; Stage 2 – audio amplifiers; and Stage 3 – automotive ignition coil transformers.

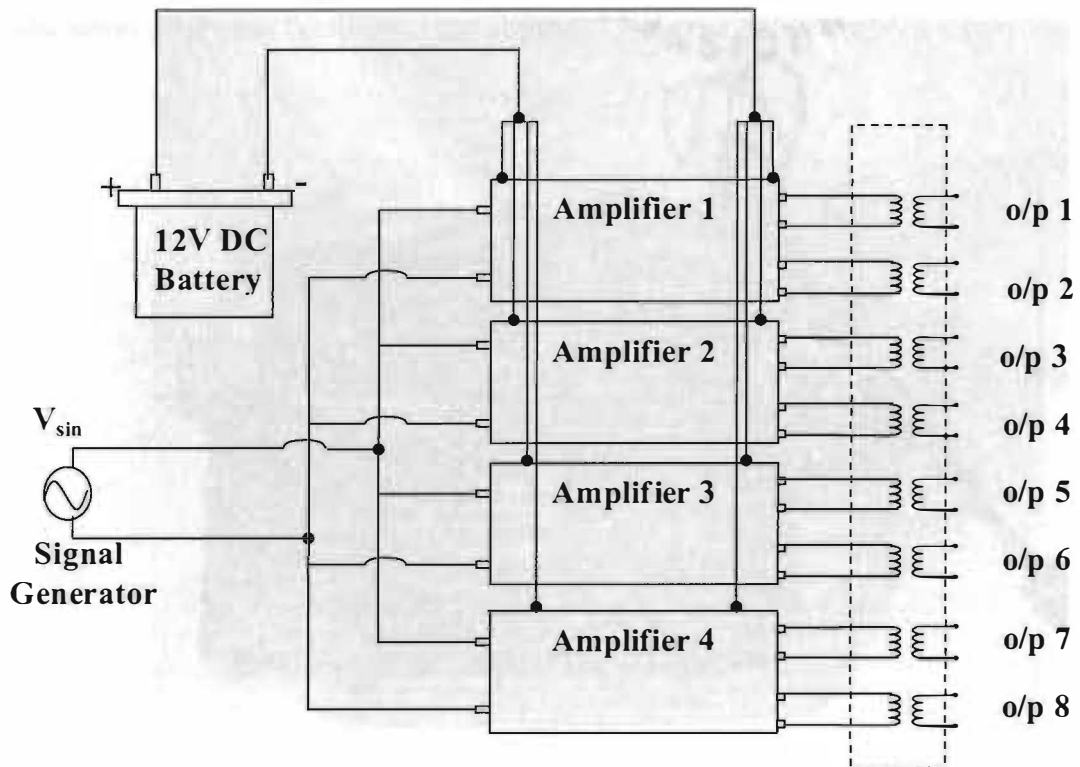


Figure 5.5 Schematic for the power supply system.

At Stage 1, four signals from the polyphase signal generator are supplied to the audio amplifiers, where the latter are driven by a 12V DC battery. Since the amplifiers have dual output channels, eight amplified signals are obtained at Stage 2. At Stage 3, the automotive ignition coil transformers produce eight polyphase high voltage signals that provide the RF high voltage for the actuators on the plasma panel. Figure 5.6 is a digital image of the experimental set-up.

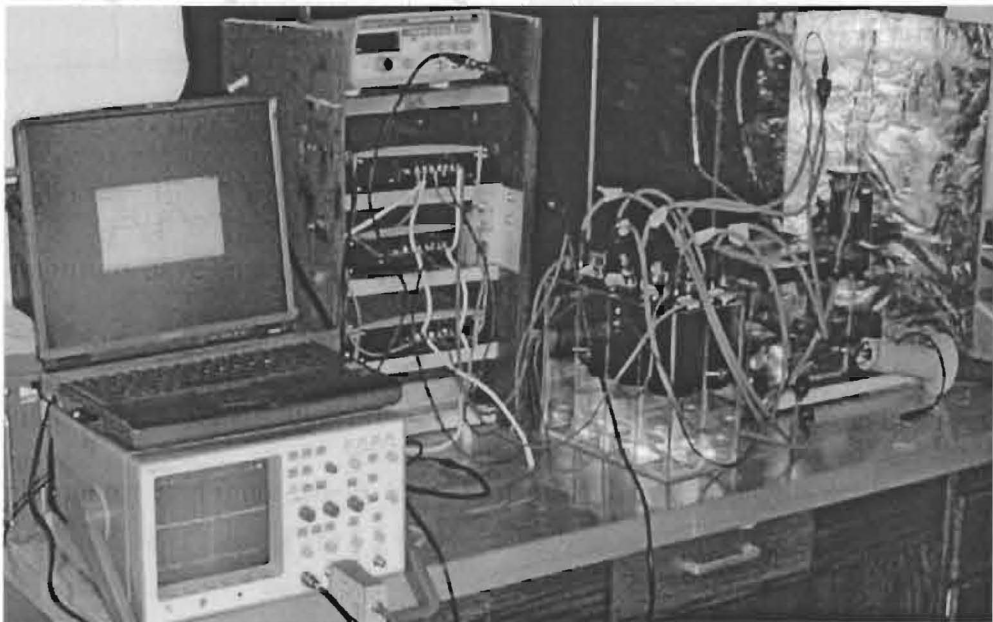


Figure 5.6 Experimental configuration for the power supply system.

5.3 Experimental Results

Using the power supply discussed in Section 5.2, several tests were run using the paraelectric panel, shown in Figure 5.7a under normal illumination. For these experiments, a PC board panel was preferred over the ceramic panels discussed in Chapter 2, because the latter are more brittle. PC board panels have experimentally been proven to withstand higher voltages for longer periods without breakdown. It was experimentally shown that this power supply is capable of generating OAUGDP over the panel surface. The plasma generated was uniform and without filamentation. Figure 5.7b is a digital image of the panel energized with a voltage of 4 kV and a frequency of 4 kHz.

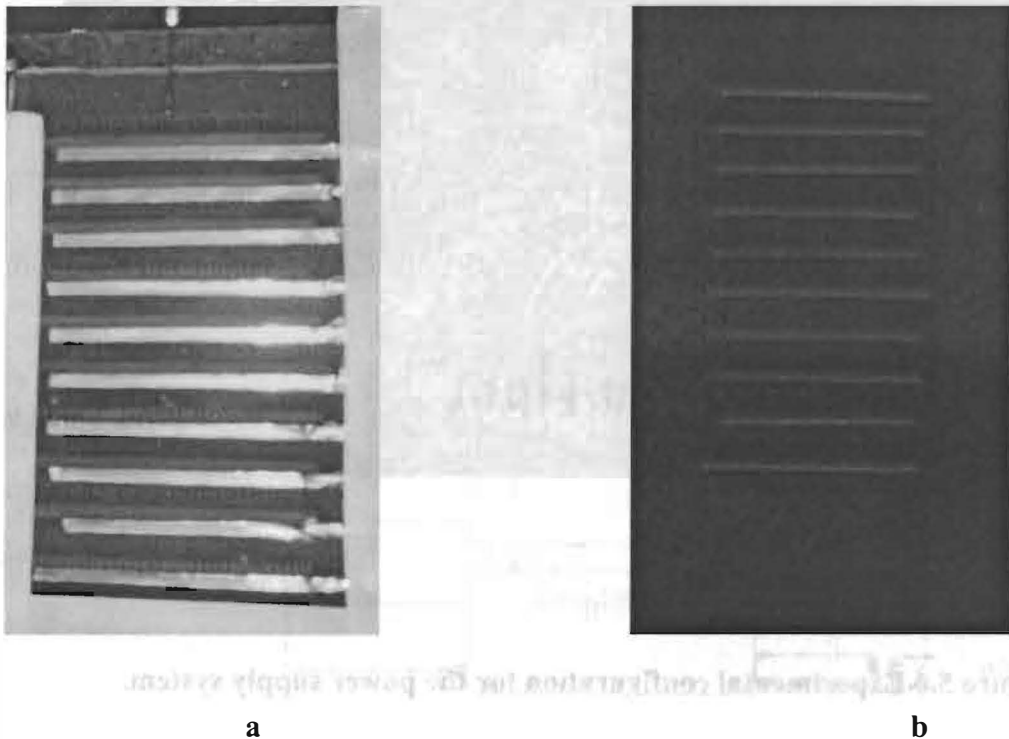


Figure 5.7 OAUGDP[®] actuator panels. (a) Plasma panel under normal illumination. (b) Plasma panel energized by the low cost power supply.

The experimental results are plotted in Figure 5.8 [21]. As is clear from the graph, this power supply is capable of producing results comparable to those obtained with the conventional power supply.

5.4 Advantages of the Low Cost Power Supply

The power supply discussed in this chapter has several operational advantages over the conventional power supply discussed in Section 3.1, as follows:

1. Transportation issues:

The power supply shown in Figure 3.1 consists of four high voltage transformers and four amplifiers, which make it heavy and bulky. It is cumbersome and inconvenient to move this power supply when required. Also,

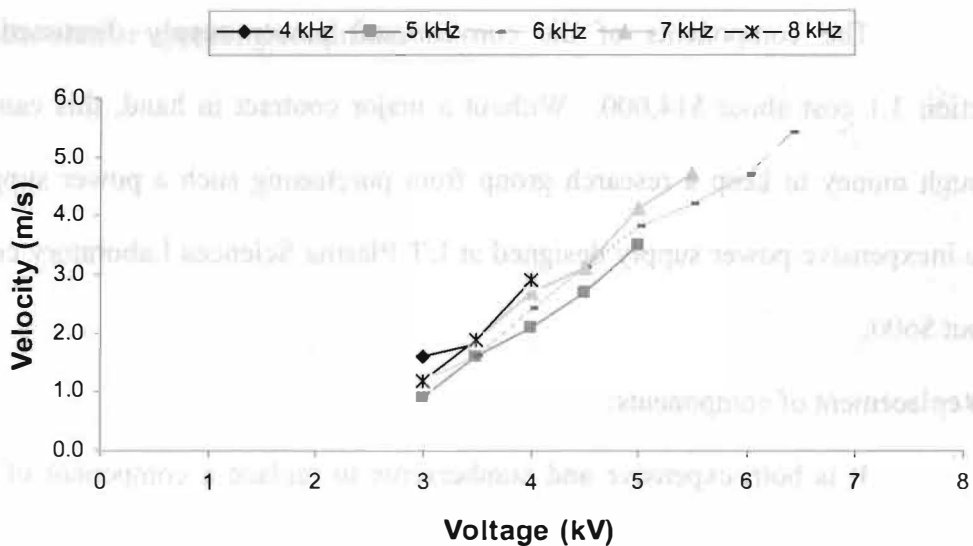


Figure 5.8 Effect of applied voltage and frequency on the flow velocity.

the transformer oil needs to be suctioned out and then refilled before and after a move, since it would otherwise slosh out whenever the power supply is transported in a vehicle. This problem was encountered when the power supply was moved to the NASA Langley Research Center for the research campaign conducted in May 2003. The low cost power supply solves this problem because it is lightweight and convenient to move.

2. Maintenance and troubleshooting issues:

It is difficult to both identify and diagnose the problem whenever any operational problem arises with the conventional power supply. The low cost power supply designed to replace the conventional technology consists of automotive ignition coils and audio amplifiers, so the individual components can be removed and checked for problems without much difficulty.

3. Cost:

The components of the conventional power supply discussed in Section 3.1 cost about \$14,000. Without a major contract in hand, this can be enough money to keep a research group from purchasing such a power supply. The inexpensive power supply designed at UT Plasma Sciences Laboratory costs about \$600.

4. Replacement of components:

It is both expensive and cumbersome to replace a component of the conventional power supply, be it a transformer or an amplifier. On the other hand, the individual components of the low-cost power supply are both easy and

economical to replace. A typical automotive ignition coil and an audio amplifier cost about \$20 and \$75 respectively. Also, it takes considerably less time to make such a replacement in the low cost design, since the automotive ignition coils and the audio amplifiers are easily available off-the-shelf at any automobile service shop.

5. Operational Parameters:

Though not as high, the voltage and frequency ratings of the low cost power supply are close to that of the conventional power supply. The low cost power supply is capable of producing voltages up to 7 kV and a frequency as high as 10 kHz. It was observed that the audio amplifier + ignition coil system performs satisfactorily for a wide range of frequency without overheating [18]. This power supply was capable of energizing the plasma actuators and produced similar results to that produced by the conventional Powertron™ power supply under similar operating conditions.

6. SUMMARY AND DISCUSSION

The ability of plasma actuators to manipulate the boundary layer velocity profiles and to produce aerodynamic acceleration was demonstrated. Velocities up to several meters per second were obtained at one atmosphere using piezoelectric and peristaltic OAUGDP actuators. Though desirable velocities are of the order of approximately 50 m/sec, which is the take-off and landing speed of the aircrafts, this work illustrates that with some additional adjustments, velocities of that order might be possible.

Smoke flow visualization tests were conducted to demonstrate the boundary layer turbulence for various panel configurations discussed in chapter 2. A pure peristaltic panel configuration has the disadvantage of piezoelectrically induced flow counteracting the flow generated by peristaltic waves. It was illustrated that combined piezoelectric and peristaltic panel can be used to have the piezoelectrically induced flow add to the flow induced by peristaltic wave.

A low cost power supply to energize the piezoelectric panel was built in the UT Plasma Laboratory. This power supply was proved to be cheaper, easier to troubleshoot and maintain, and easier to transport. The experimental results obtained using the economical power supply were demonstrated. These results were comparable to the ones obtained using the conventional power supply.

REFERENCES

1. M. J. B. Cantwell, "The Flow of a Gas from a Nozzle into a Chamber," *Journal of Applied Physics*, Vol. 37, No. 12, pp. 3681-3688, 1966.
2. J. H. Van Dyke, "The Flow of a Gas from a Nozzle into a Chamber," *Journal of Applied Physics*, Vol. 37, No. 12, pp. 3689-3696, 1966.
3. J. H. Van Dyke, "The Flow of a Gas from a Nozzle into a Chamber," *Journal of Applied Physics*, Vol. 37, No. 12, pp. 3697-3704, 1966.
4. J. H. Van Dyke, "The Flow of a Gas from a Nozzle into a Chamber," *Journal of Applied Physics*, Vol. 37, No. 12, pp. 3705-3712, 1966.
5. J. H. Van Dyke, "The Flow of a Gas from a Nozzle into a Chamber," *Journal of Applied Physics*, Vol. 37, No. 12, pp. 3713-3720, 1966.
6. J. H. Van Dyke, "The Flow of a Gas from a Nozzle into a Chamber," *Journal of Applied Physics*, Vol. 37, No. 12, pp. 3721-3728, 1966.
7. J. H. Van Dyke, "The Flow of a Gas from a Nozzle into a Chamber," *Journal of Applied Physics*, Vol. 37, No. 12, pp. 3729-3736, 1966.
8. J. H. Van Dyke, "The Flow of a Gas from a Nozzle into a Chamber," *Journal of Applied Physics*, Vol. 37, No. 12, pp. 3737-3744, 1966.
9. J. H. Van Dyke, "The Flow of a Gas from a Nozzle into a Chamber," *Journal of Applied Physics*, Vol. 37, No. 12, pp. 3745-3752, 1966.
10. J. H. Van Dyke, "The Flow of a Gas from a Nozzle into a Chamber," *Journal of Applied Physics*, Vol. 37, No. 12, pp. 3753-3760, 1966.

REFERENCES

1. Roth, J. R.: "Industrial Plasma Engineering. Volume I – Principles"- Institute of Physics Publishing, Bristol and Philadelphia, ISBN 0-7503-0318-2, (1995).
2. Roth, J. R.: "Industrial Plasma Engineering. Volume II -- Applications to Non-Thermal Plasma Processing"- Institute of Physics Publishing, Bristol and Philadelphia, ISBN 0-7503-0545-2, (2001). (8)
3. Von Eagle, A., Seeliger, R, and Steenback, M.: "On the Glow Discharge at High Pressure" - Zeit. fur Physik Vol. 85, 144 (1933) pp 140-160.
4. Roth J. R., Tsai P. P., Liu C., Laroussi M. and Spence P. D.: "One Atmosphere Uniform Glow Discharge Plasma"- U. S. Patent #5,414,324, Issued May 9, 1995.
5. Massines, F.; Ben Gadri, R.; Rabehi, A.; Decomps, Ph.; Segur, P.; and Mayoux, Ch.: "Experimental and Theoretical Study of a Glow Discharge at Atmospheric Pressure Controlled by Dielectric Barrier"- Journal of Applied Physics, vol. 83, No. 6, pp 2950-2957, 1998.
6. Ben Gadri R.: "One Atmosphere Glow Discharge Structure Revealed by Computer Modeling"- IEEE Trans. Plasma Sci., Vol. 27, No. 1, 1999.
7. Sherman, D. M.: "Manipulating Aerodynamic Boundary Layers Using an Electrohydrodynamic Effect Generated by a One Atmosphere Uniform Glow Discharge Plasma"- M. S. in Physics Thesis, Department of Physics, University of Tennessee, Knoxville, August 1998.

8. Sherman D. M., Wilkinson S. P., and Roth J. R.: "Paraelectric Gas Flow Accelerator"- U. S. Patent # 6,200,539 B1, Issued March 13, 2001.
9. Roth J. R.: "Method and Apparatus for Covering Bodies with a Uniform Glow Discharge Plasma and Applications Thereof"- U. S. Patent #5,669,583, Issued Sept 23, 1997.
10. Sin H., Madhan R., Roth J. R. and Wilkinson S.: "Subsonic Plasma Aerodynamics using Lorentzian Momentum Transfer in Atmospheric Normal Glow Discharge Plasmas"- Paper YF2- 004, Presented at the 55th APS Gaseous Electronics Conference, Minneapolis, Minnesota, October 15-18, 2002, APS Bulletin, Volume 47, No.- 07 (2002), Page -78.
11. Roth J. R., Sherman D. M. and Wilkinson S. P.: "Boundary Layer Flow Control with a One Atmosphere Uniform Glow Discharge Surface Plasma"- AIAA Paper 98-0328, Proc. of the 36th AIAA Aerospace Sciences Meeting & Exhibit Reno, NV, January 12-15, 1998.
12. W. Shyy, B. Jayaraman and A. Anderson: "Modeling of Glow Discharge-induced Fluid Dynamics"- Journal of Applied Physics, Vol. 92, No. 11 (2002) pp 6434- 6443.
13. Roth J. R.: "Aerodynamic Flow Acceleration using Paraelectric and Peristaltic Electrohydrodynamic (EHD) Effects of a One Atmosphere Uniform Glow Discharge Plasma (OAUGDP[®])"- Physics of Plasmas, Vol. 10, No.5 (2003).
14. PCI/PXI-6711/6713 User Manual, National Instruments, October 1998 Edition Part Number 322080A-01.

15. Madhan R.C.M. "Boundary Layer Flow Acceleration by Paraelectric and Peristaltic EHD Effects of Aerodynamic Plasma Actuators"- M.S. in Electrical Engineering Thesis, Department of Electrical and Computer Engineering, University of Tennessee, Knoxville, May 2004.
16. Roth J. R., Sherman D. M. and Wilkinson S. P.: "Electrohydrodynamic Flow Control with a Glow Discharge Surface Plasma"- AIAA Journal, Vol. 38, No. 7, July 2000, pp 1166-1172.
17. Roth J. R., Madhan R., Rahel J. and Yadav M. "Aerodynamic Boundary Layer Control Using EHD Effects of a One Atmosphere Uniform Glow Discharge Plasma (OAUGDP[®])"- Paper GTP 024, Proceedings of the 2003 APS Gaseous Electronics Conference, October 21-24, 2003, San Francisco, California.
18. Roth J. R., Madhan, R. C. M., Manish Yadav, Jozef Rahel and Wilkinson S. P.: "Flow Field Measurement of Paraelectric, Peristaltic and Combined Plasma Actuators based on the One Atmosphere Uniform Glow Discharge Plasma (OAUGDP[™])"- AIAA Paper 2003-0845, Presented at the 42nd AIAA Aerospace Sciences Meeting & Exhibit Reno, NV, January 5-8, 2004.
19. Roth J.R., Yadav M., Madhan R. and Wilkinson S.: "Aerodynamic Flow Control by Peristaltic Acceleration of a One Atmosphere Uniform Glow Discharge Plasma"- Paper 5A07, Proceedings of the 30th IEEE International Conference on Plasma Science, Jeju, Korea, June 2-5, 2003, Page 320, IEEE Catalog Number 03CH37470, ISBN 0-7803-7911-X.

20. User Manual – 2004 Edition, Brilliant Electronics (http://www.brilliant-electronics.com/car_amplifiers_spl_crm300_2.htm).
21. Manish Yadav, Xin Dai and Roth J. R.: "Measurement of the Boundary Layer Velocity Induced by Paraelectric Plasma Actuators using an Inexpensive High Voltage Power Supply"- Paper 3P-38, Proceedings of the 31st IEEE International Conference on Plasma Science, Baltimore, Maryland, June 28-July 1, 2004, Page 244, IEEE Catalog No. 04CH37537, ISBN 0-7803-8334-6.

VITA

Manish Yadav received his Bachelor of Engineering degree (with distinction) from Jawaharlal Institute of Technology, Khargone, India in June, 2001. There, he was the first rank holder in the department for eight consecutive semesters. He began his graduate studies in Electrical Engineering at the University of Tennessee, Knoxville as a graduate research assistant in the UT Plasma Sciences Laboratory. He has worked in the field of subsonic plasma aerodynamics, using the One Atmosphere Uniform Glow Discharge Plasma (OAUGDP[®]) to cause aerodynamic flow acceleration and manipulation of the boundary layer. In addition to industrial applications of plasma science, his research interests include VLSI design and computer networking. He is a student member of the IEEE Nuclear and Plasma Sciences Society. He plans to join the MBA program after graduating from the Department of Electrical and Computer Engineering in Summer – 2005.

4533 0543 9
11/09/05 MAB